

EXPERIMENTAL ASPECTS OF PLATINUM-GROUP MINERALS

10

Anna Vymazalová¹ and Dmitriy A. Chareev²

¹Czech Geological Survey, Prague, Czech Republic ²Institute of Experimental Mineralogy RAS, Chernogolovka, Russia

CHAPTER OUTLINE

10.1 Introduction	304
10.2 Experimental Methods for Synthesis of Platinum-Group Minerals.....	314
10.3 Powder Samples	314
10.3.1 Dry Technique	314
10.4 Single Crystals.....	316
10.4.1 Congruent Techniques.....	316
10.4.2 Incongruent Techniques	317
10.4.3 PGE-Bearing Crystals Prepared by Flux Technique	320
10.5 Platinum-Group Minerals and Synthetic Analogues.....	324
10.5.1 Bortnikovite Pd ₄ Cu ₃ Zn	326
10.5.2 Coldwellite Pd ₃ Ag ₂ S	327
10.5.3 Ferhodsite (Fe,Rh,Ni,Ir,Cu,Pt) ₉ S ₈	328
10.5.4 Jacutingaite Pt ₂ HgSe ₃	328
10.5.5 Jaguéite Cu ₂ Pd ₃ Se ₄	329
10.5.6 Kalungaite PdAsSe	330
10.5.7 Kingstonite Rh ₃ S ₄	331
10.5.8 Kitagohaita Pt ₇ Cu.....	331
10.5.9 Kojonenite Pd _{7-x} SnTe ₂ (0.3 ≤ x ≤ 0.8).....	332
10.5.10 Lisiguangite CuPtBiS ₃	333
10.5.11 Lukkulaisvaaraite Pd ₁₄ Ag ₂ Te ₉	334
10.5.12 Malyshevite PdCuBiS ₃	335
10.5.13 Miessiite Pd ₁₁ Te ₂ Se ₂	336
10.5.14 Milotaite PdSbSe	337
10.5.15 Naldrettite Pd ₂ Sb.....	338
10.5.16 Nielsenite PdCu ₃	339
10.5.17 Norilskite (Pd,Ag) ₇ Pb ₄	340
10.5.18 Palladosilicide Pd ₂ Si	341
10.5.19 Pašavaite Pd ₃ Pb ₂ Te ₂	342
10.5.20 Skagaardite PdCu	342

10.5.21 Törnroosite $Pd_{11}As_2Te_2$	343
10.5.22 Ungavaite Pd_4Sb_3	344
10.5.23 Zaccariniite $RhNiAs$	345
Acknowledgements	346
References	346

10.1 INTRODUCTION

The Platinum-group elements (PGEs) are of significant technological importance. PGEs are used primarily in industrial applications (e.g., catalysts) and have become widely established in chemical, electrical, and electronic engineering. The PGEs and the compounds they form have attracted considerable attention in recent years due to their specific properties and their application in new technologies. They exhibit various interesting physical, chemical, and structural properties that place these compounds at the interface of chemistry, mineralogy, solid-state physics, and material science. Therefore, there is still a demand for exploration and mining and to advance the understanding of the natural process that lead to their formation.

This chapter consolidates the experimental methods that can be applied for the synthesis of PGE compounds. Dry synthesis and the major experimental methods used to try to obtain single crystals are summarized and some examples of the synthesis of PGE phases are discussed. A list of approved platinum-group minerals (PGMs) recognized up to the end of 2016, is presented with a focus on newly-named minerals and their experimental aspects. The up-to-date list of recognized PGMs is given in [Tables 10.1–10.3](#). This chapter is written to encourage the application of experimental studies for a better understanding of PGM, their formation and occurrence under natural conditions. The available knowledge is often dispersed across the chemical, physical, mineralogical, and metallurgical literature. Additionally, there is often an information gap between investigations of synthetic systems and those of natural minerals. A number of PGE-bearing compounds have been determined and studied due to their specific (e.g., electrical or electrochemical) properties rather than their mineralogical significance.

There is a wide range of data on the unary and binary systems available in the literature (e.g., a compendium of binary diagrams by [Massalski, 1990](#)). The systems containing PGEs were consolidated by [Berlincourt et al. \(1981\)](#), who thoroughly summarized the unary, binary, and ternary systems with PGEs. Later, [Makovicky \(2002\)](#) reported on further ternary and quaternary systems containing PGE. Since then, a few other ternary and quaternary systems of mineralogical significance containing PGEs were covered, involving Os, Pd, Pt, and Rh (Os-Mo-S: [Drábek and Rieder, 2008](#); Pd-Ag-Te: [Vymazalová et al., 2015](#); Pd-Ag-Se: [Vymazalová et al., 2014b](#); Pd-Hg-Se: [Drábek et al., 2014](#); Pd-Pb-Te: [Vymazalová and Drábek, 2011](#); Pd-Sn-Te: [Vymazalová and Drábek, 2010](#); Pd-Cu-Se: [Makovicky and Karup-Møller, in press](#); Pd-Cu-Fe-S: [Karup-Møller et al., 2008](#); Pd-Ni-Fe-S: [Makovicky and Karup-Møller, 2016](#); Pd-Pt-Sb: [Kim, 2009](#); Pd-Pt-Ni-Te: [Helmy et al., 2007](#); Pt-Hg-Se: [Drábek et al., 2012](#); Rh-Cu-S: [Karup-Møller and Makovicky, 2007](#)). Nevertheless, as emphasized by [Makovicky \(2002\)](#) there is still a need to cover additional phase systems important for PGE deposits. Particularly unresearched are systems containing phases that are less common but of mineralogical significance and potentially of an economic importance (e.g., Pd-As-Sn,

Table 10.1 Platinum-Group Minerals (Ideal Formulas)

Name	Formula	Name	Formula	Name	Formula
Anduoite	RuAs ₂	Ferrorhodsite	FeRh ₂ S ₄	Kojonenite ^a	Pd _{7-x} SnTe ₂
Arsenopalladinite	Pd ₈ As _{2.5} Sb _{0.5}	Froodite	PdBi ₂	Konderite	Cu ₃ PbRh ₈ S ₁₆
Atheneite	Pd ₂ As _{0.75} Hg _{0.25}	Gaotaiite	Ir ₃ Te ₈	Kotulskite	PdTe
Atokite	Pd ₃ Sn	Genkinite	(Pt,Pd) ₄ Sb ₃	Kravtsovite ^a	PdAg ₂ S
Borovskite	Pd ₃ SbTe ₄	Geversite	PtSb ₂	Laflammeite	Pd ₃ Pb ₂ S ₂
Bortnikovite ^a	Pd ₄ Cu ₃ Zn	Hexaferrum	(Fe,Ru,Os,Ir)	Laurite	RuS ₂
Bowieite	Rh ₂ S ₃	Hollingworthite	RhAsS	Lisiguangite ^a	CuPtBiS ₃
Braggite	(Pt,Pd)S	Hongshiite	PtCu	Luberoite	Pt ₅ Se ₄
Cabriite	Pd ₂ SnCu	Inaglyite	Cu ₃ PbIr ₈ S ₁₆	Lukkulaisvaaraite ^a	Pd ₁₄ Ag ₂ Te ₉
Changchengite	IrBiS	Insizwaite	PtBi ₂	Majakite	PdNiAs
Chengdeite	Ir ₃ Fe	Irarsite	IrAsS	Malanite	CuPt ₂ S ₄
Cherepanovite	RhAs	Iridarsenite	IrAs ₂	Malyshevite ^a	PdCuBiS ₃
Chrisstanleyite	Ag ₂ Pd ₃ Se ₄	Iridium	Ir	Marathonite ^a	Pd ₂₅ Ge ₉
Coldwellite ^a	Pd ₃ Ag ₂ S	Isoferroplatinum	Pt ₃ Fe	Maslovite	PtBiTe
Cooperite	PtS	Isomertieite	Pd ₁₁ Sb ₂ As ₂	Mayingite	IrBiTe
Crerarite	(Pt,Pb)Bi ₃ S _{4-x}	Jacutingaite ^a	Pt ₂ HgSe ₃	Menshikovite	Pd ₃ Ni ₂ As ₃
Cuproiridsite	CuIr ₂ S ₄	Jaguéite ^a	Cu ₂ Pd ₃ Se ₄	Merenskyite	PdTe ₂
Cuprorhodsite	CuRh ₂ S ₄	Kalungaite ^a	PdAsSe	Mertieite I	Pd ₁₁ (Sb,As) ₄
Damiaoite	PtIn ₂	Kashinite	Ir ₂ S ₃	Mertieite II	Pd ₈ Sb _{2.5} As _{0.5}
Daomanite	PtCuAsS ₂	Keithconnite	Pd ₂₀ Te ₇	Miessiite ^a	Pd ₁₁ Te ₂ Se ₂
Erlichmanite	OsS ₂	Kharelakhite	(Cu,Fe) ₄ (Pt,Pb) ₄ NiS ₈	Michenerite	PdBiTe
Ferhodsite ^a	(Fe,Rh,Ni,Ir,Cu,Pt) ₉ S ₈	Kingstonite ^a	Rh ₃ S ₄	Milotait ^a	PdSbSe
Ferronickelplatinum	PtFe _{0.5} Ni _{0.5}	Kitagohait ^a	Pt ₇ Cu	Moncheite	PtTe ₂

(Continued)

Table 10.1 Platinum-Group Minerals (Ideal Formulas) *Continued*

Name	Formula	Name	Formula	Name	Formula
Naldrettite ^a	Pd ₂ Sb	Polarite	PdBi	Taimyrite	(Pd,Cu) ₃ Sn
Nielsenite ^a	PdCu ₃	Polkanovite	Rh ₁₂ As ₇	Tatyanaite	Pt ₉ Cu ₃ Sn ₄
Niggliite	PtSn	Potarite	PdHg	Telargpalite	Pd _{2-x} Ag _{1+x} Te
Norilskite ^a	(Pd,Ag) ₇ Pb ₄	Prassoite	Rh ₁₇ S ₁₅	Telluropalladinite	Pd ₉ Te ₄
Omeite	OsAs ₂	Rhodarsenide	(Rh,Pd) ₂ As	Temagamite	Pd ₃ HgTe ₃
Oosterboschite	(Cu,Pd) ₇ Se ₅	Rhodium	Rh	Testibiopalladite	PdSbTe
Osarsite	OsAsS	Rhodplumsite	Rh ₃ Pb ₂ S ₂	Tetraferroplatinum	PtFe
Osmium	Os	Ruarsite	RuAsS	Tischendorfite	Pd ₈ Hg ₃ Se ₉
Oulankaite	Pd ₅ Cu ₄ SnTe ₂ S ₂	Rustenburgite	Pt ₃ Sn	Tolovkite	IrSbS
Padmaite	PdBiSe	Ruthenarsenite	RuAs	Törnroosite ^a	Pd ₁₁ As ₂ Te ₂
Palarstanide	Pd ₅ (Sn,As) ₂	Rutheniridosmine	(Ir,Os,Ru)	Tulameenite	PtFe _{0.5} Cu _{0.5}
Palladium	Pd	Ruthenium	Ru	Ungavaite ^a	Pd ₄ Sb ₃
Palladoarsenide	Pd ₂ As	Shungfengite	IrTe ₂	Urvantsevite	Pd(Bi,Pb) ₂
Palladobismutharsenide	Pd ₂ As _{0.8} Bi _{0.2}	Skaergaardite ^a	PdCu	Vasilite	Pd ₁₆ S ₇
Palladodymite	(Pd,Rh) ₂ As	Sobolevskite	PdBi	Verbeekite	PdSe ₂
Palladgermanide ^a	Pd ₂ Ge	Sopcheite	Ag ₄ Pd ₃ Te ₄	Vincentite	(Pd,Pt) ₃ (As,Sb,Te)
Palladosilicide ^a	Pd ₂ Si	Sperrylite	PtAs ₂	Vymazalováite ^a	Pd ₃ Bi ₂ S ₂
Palladseite	Pd ₁₇ Se ₁₅	Stannopalladinite	Pd ₅ Sn ₂ Cu	Vysotskite	PdS
Palovite	Pd ₂ Sn	Stibiopalladinite	Pd _{5+x} Sb _{2-x}	Yixunite	Pt ₃ In
Pašavaite ^a	Pd ₃ Pb ₂ Te ₂	Stillwaterite	Pd ₈ As ₃	Zaccariniite ^a	RhNiAs
Platarsite	PtAsS	Stumpflite	PtSb	Zvyagintsevite	Pd ₃ Pb
Platinum	Pt	Sudburyite	PdSb		
Plumbopalladinite	Pd ₃ Pb ₂	Sudovikovite	PtSe ₂		

^aNew minerals described from 2002 to 2016.

Table 10.2 Revised Platinum-Group Minerals, Crystallographic Data

Mineral		Crystallographic Data		Unit Cell Parameters						Reference
Name	Formula	Space group		a (Å)	b (Å)	c (Å)	β (°)	V(Å³)	Z	
Atheneite	Pd ₂ As _{0.75} Hg _{0.25}	Hexagonal	<i>P</i> 6/2 <i>m</i>	6.813		3.4892		140.26	3	Bindi (2010)
Chrisstanleyite	Ag ₂ Pd ₃ Se ₄	Monoclinic	<i>P</i> 2 ₁ / <i>c</i>	5.676	10.342	6.341	114.996	337.3	2	Topa et al. (2006)
Mertieite II	Pd ₈ Sb _{2.5} As _{0.5}	Trigonal	<i>R</i> 3 <i>ch</i>	7.5172		43.037		2106.1	12	Karimova et al. (in press)
Sopcheite	Ag ₄ Pd ₃ Te ₄	Orthorhombic	<i>Cmca</i>	12.212	6.138	12.234		917.1	4	Laufek et al. (in press)
Temagamite ^a	Pd ₃ HgTe ₃	Hexagonal	<i>P</i> 3 <i>m</i> 1	7.8211		17.281		917.8	6	Laufek et al. (2016)
Tischendorfite ^a	Pd ₈ Hg ₃ Se ₉	Orthorhombic	<i>Pmmm</i>	7.1886	16.8083	6.4762		782.51	2	Laufek et al. (2014)

^aCrystal structure solved from the synthetic analogue.

Table 10.3 Platinum-Group Minerals, Described Since 2002 and Their Crystallographic Data

Name	Formula	Crystal Structure Data		Unit Cell Parameters				V (Å³)	Z	Reference
		Space Group		a (Å)	b (Å)	c (Å)	β (°)			
Bortnikovite	Pd ₄ Cu ₃ Zn	Tetragonal	P4/ mmm ?	6.00		8.50		306.0	3	Mochalov et al. (2007)
Coldwellite	Pd ₃ Ag ₂ S	Cubic	P4 ₃ 32	7.2470				380.61	4	McDonald et al. (2015)
Ferhdsite	(Fe,Rh,Ni, Ir,Cu,Pt) ₉ S ₈	Tetragonal	?	10.009		9.840		985.77		Begizov (2009) ^a
Jacutingaite	Pt ₂ HgSe ₃	Trigonal	P $\bar{3}$ m1	7.3477		5.2955		247.59	2	Vymazalová et al. (2012a)
Jaguéite	Cu ₂ Pd ₃ Se ₄	Monoclinic	P2 ₁ /c	5.672	9.910	6.264	115.40	318.1	2	Paar et al. (2004), Topa et al. (2006)
Kalungaite	PdAsSe	Cubic	Pa $\bar{3}$	6.089				225.78	4	Botelho et al. (2006)
Kingstonite	Rh ₃ S ₄	Monoclinic	C2/m	10.4616	10.7527	6.2648	109.0	666.34	6	Stanley et al. (2005)
Kitagohait	Pt ₇ Cu	Cubic	Fm $\bar{3}$ m	7.7891				472.57	4	Cabral et al. (2014)
Kojonenite	Pd _{7-x} SnTe ₂	Tetragonal	I4/ mmm	4.001		20.929		335.0	2	Stanley and Vymazalová (2015)
Kravtsovite	PdAg ₂ S	Orthorhombic	Cmcm	7.9835	5.9265	5.7451		271.82	4	Vymazalová et al. (in press)
Lisiguangite	CuPtBiS ₃	Orthorhombic	P2 ₁ 2 ₁ 2 ₁	7.7152	12.838	4.9248		487.80	4	Yu et al. (2009)
Lukkulaisvaaraite	Pd ₁₄ Ag ₂ Te ₉	Tetragonal	I4/m	8.9599		11.822		949.1	2	Vymazalová et al. (2014a)
Malyshevite	PdCuBiS ₃	Orthorhombic	Pnam	7.541	6.4823	11.522		563.204	4	Chernikov et al. (2006)
Marathonite	Pd ₂₅ Ge ₉	Trigonal	P3	7.391		10.477		495.65	1	McDonald et al. (2016)
Miessite	Pd ₁₁ Te ₂ Se ₂	Cubic	Fd3m	12.448				1929.0	8	Kojonen et al. (2007)
Milotaite	PdSbSe	Cubic	P2 ₁ 3	6.3181				252.20	4	Paar et al. (2005)
Naldrettite	Pd ₂ Sb	Orthorhombic	Cmc2 ₁	3.3906	17.5551	6.957		414.097	8	Cabri et al. (2005)

Nielsenite	PdCu ₃	Tetragonal	<i>P</i> 4 <i>mm</i>	3.7125		25.62		353.2	4	McDonald et al. (2008)
Norilskite	(Pd, Ag) ₇ Pb ₄	Trigonal	<i>P</i> 3 ₁ 21	8.9656		17.2801		1202.92	6	Vymazalová et al. (2017)
Palladogermanide	Pd ₂ Ge	Hexagonal	<i>P</i> 6̄2 <i>m</i>	6.712		3.408		132.96	3	McDonald et al. (2017b)
Palladosilicide	Pd ₂ Si	Hexagonal	<i>P</i> 6̄2 <i>m</i>	6.496		3.433		125.5	3	Cabri et al. (2015)
Pašavaite	Pd ₃ Pb ₂ Te ₂	Orthorhombic	<i>P</i> mmm	8.599	5.9381	6.3173		322.6	2	Vymazalová et al. (2009)
Skaergaardite	PdCu	Cubic	<i>P</i> m3 <i>m</i>	3.0014				27.0378	1	Rudashevsky et al. (2004)
Törnroosite	Pd ₁₁ As ₂ Te ₂	Cubic	<i>F</i> d̄3 <i>m</i>	12.3530				1885.03	8	Kojonen et al. (2011)
Ungavaite	Pd ₄ Sb ₃	Tetragonal	?	7.7388		24.145		1446.02	8	McDonald et al. (2005)
Vymazalováite	Pd ₃ Bi ₂ S ₂	Cubic	<i>I</i> 2 ₁ 3	8.3097				573.79	4	Sluzhenikin et al. (in press)
Zaccariniite	RhNiAs	Tetragonal	<i>P</i> 4/ <i>nmm</i>	3.5498		6.1573		77.59	2	Vymazalová et al. (2012b)

^aNo further data available.

Table 10.4 Experimental Data for Ternary Systems and the Corresponding PGM (Ideal Formulae)

System	Mineral Name	Formula	Type of Diagram, at T ($^{\circ}\text{C}$)	Compositional Range	Reference
Ir-As-S	Irarsite	IrAsS	None		
Ir-Bi-S	Changchengite	IrBiS	None		
Ir-Bi-Te	Mayingite	IrBiTe	None		
Ir-Cu-S	Cuproiridsite	CuIr ₂ S ₄	None		
Ir-Sb-S	Tolovkite	IrSbS	None		
Os-As-S	Osarsite	OsAsS	None		
Pd-Ag-Pb	Norilskite	(Pd,Ag) ₇ Pb ₄	Isothermal section, 400	Full	Sarah et al. (1981)
Pd-Ag-S	Coldwellite	Pd ₃ Ag ₂ S	Isothermal section, 400, 550	Full	Vymazalová et al., in prep.
	Kravtsovite	PdAg ₂ S	Vertical section, 400–1600	Partial, Ag ₂ S-Pd	Raub (1954)
Pd-Ag-Se	Chrisstanleyite	Ag ₂ Pd ₃ Se ₄	Isothermal section, 350, 430, 530	Full	Vymazalová et al. (2014b)
Pd-Ag-Te	Lukkulaisvaaraite	Pd ₁₄ Ag ₂ Te ₉	Isothermal section, 350, 450	Full	Vymazalová et al. (2015)
	Sopcheite	Ag ₄ Pd ₃ Te ₄	Vertical section, 0–1000	Partial, Ag _{22.2} Pd _{66.6} Te _{11.2} -Ag _{66.7} Te _{33.3}	Chernyaev et al. (1968)
Pd-As-Bi	Telargpalite	Pd _{2-x} Ag _{1+x} Te		Partial, As-Bi-Bi ₅₀ Pd ₅₀ - As ₁₅ Bi ₃₅ Pd ₅₀ -As ₃₃ Pd ₆₇ -As ₂₅ Pd ₇₅ - Bi ₂₅ Pd ₇₅ -Pd	El-Boragy and Schubert (1971a)
	Palladobismutharsenide	Pd ₂ As _{0.8} Bi _{0.2}	Isothermal section, 400	Partial, Pd _{1.97} As _{0.80} Bi _{0.23} - Pd ₂ As	Cabri et al. (1976)
Pd-As-Hg	Atheneite	Pd ₂ As _{0.75} Hg _{0.25}	None		
Pd-As-Sb	Arsenopalladinite	Pd ₈ As _{2.5} Sb _{0.5}	Isothermal section,		
	Isomertieite	Pd ₁₁ Sb ₂ As ₂	710		
	Mertieite I	Pd ₁₁ (Sb,As) ₄			
	Mertieite II	Pd ₈ Sb _{2.5} As _{0.5}			
Pd-As-Se	Kalungaite	PdAsSe	None		

Pd-As-Sn	Palarstanide	$\text{Pd}_5(\text{Sn},\text{As})_2$	Tentative isothermal section, 500 Isothermal section, 25	Partial	Pratt (1994)
Pd-As-Te	Törmroosite	$\text{Pd}_{11}\text{As}_2\text{Te}_2$	Isothermal section, 480	Partial, $\text{SnAs}-\text{Pd}_{50}\text{Sn}_{50}-\text{Sn}$ Full	El-Boragy and Schubert (1971b)
Pd-Bi-Pb	Urvantsevite	$\text{Pd}(\text{Bi},\text{Pb})_2$	Vertical section, 180–600	Partial, $\text{PdBi}_2-\text{PdPb}_2$	Zhuravlev (1976)
Pd-Bi-S	Vymazalováite	$\text{Pd}_3\text{Bi}_2\text{S}_2$	None		
Pd-Bi-Se	Padmaite	PdBiSe	None		
Pd-Bi-Te	Michenerite	PdBiTe	Isothermal section, 480	Partial, Pd-rich corner	El-Boragy and Schubert (1971b)
			Isothermal section, 480	Partial, $\text{Te}-\text{Bi}_4\text{Te}_3-\text{Bi}_{60}\text{Pd}_{40}-\text{PdTe}$	Hoffman and MacLean (1976)
Pd-Cu-Se	Jaguéite Oosterboschite	$\text{Cu}_2\text{Pd}_3\text{Se}_4$ $(\text{Cu},\text{Pd})_7\text{Se}_5$	Isothermal section, 300, 400, 550, 650	Full	Makovicky and Karup-Møller (in press)
Pd-Cu-Sn	Cabriite Stannopalladinite	Pd_2SnCu $\text{Pd}_5\text{Sn}_2\text{Cu}$ $(\text{Pd},\text{Cu})_3\text{Sn}$	None	System studied in hydrothermal chloride solutions ($\text{Pd}-\text{Sn}-\text{Cu}-\text{HCl}$) at 300 and 400 °C	Evstigneeva and Nekrasov (1980)
Pd-Cu-Zn	Taimyrite Bortnikovite	$\text{Pd}_4\text{Cu}_3\text{Zn}$	Tentative isothermal section, 800	Partial	Lebrun et al. (2007) based on data from Dobersek and Kosovinc (1989)
			Experimental points at 350 to 800	Partial	Dobersek and Kosovinc (1989)
			Isothermal section, 430	Partial, Pd-Cu region containing up to 5 at.% Zn	Schubert et al. (1955)
Pd-Hg-Se	Tischendorfite	$\text{Pd}_8\text{Hg}_3\text{Se}_9$	Isothermal section, 400	Full	Drábek et al. (2014)
Pd-Hg-Te	Temagamite	Pd_3HgTe_3	None	None	
Pd-Ni-As	Majakite	PdNiAs	Isothermal section, 450	Partial	Gerville et al. (1994)

(Continued)

Table 10.4 Experimental Data for Ternary Systems and the Corresponding PGM (Ideal Formulae) *Continued*

System	Mineral Name	Formula	Type of Diagram, at T ($^{\circ}\text{C}$)	Compositional Range	Reference
Pd-Pb-Te	Menshikovite	$\text{Pd}_3\text{Ni}_2\text{As}_3$	Isothermal section, 790	Full	
	Pašavaite	$\text{Pd}_3\text{Pb}_2\text{Te}_2$	Isothermal section, 500	Partial, $\text{NiAs}_2\text{-Ni}_5\text{As}_2\text{-Pd}_3\text{As}_2\text{-PdAs}_2$	El-Boragy et al. (1984)
			Isothermal section, 400	Partial $\text{Pd}_3\text{Pb-Pb-Te-PdTe}$	Vymazalová and Drábek (2011)
			Isothermal section, 480	Partial, Pd-rich corner	El-Boragy and Schubert (1971b)
Pd-Pb-S	Laflammeite	$\text{Pd}_3\text{Pb}_2\text{S}_2$	None		
Pd-Sb-Se	Milotaite	PdSbSe	None		
Pd-Sb-Te	Borovskite	Pd_3SbTe_4	Isothermal section, 400	Full	El-Boragy and Schubert (1971b)
			Isothermal section, 600	Full	Kim and Chao (1991)
	Testibiopalladite	PdSbTe	Isothermal section, 800	Partial, $\text{Pd-Pd}_{40}\text{Sb}_{60}\text{-Pd}_{40}\text{Te}_{60}$	
			Isothermal section, 1000	Partial, $\text{Pd}_{60}\text{Sb}_{40}\text{-Pd-Pd}_{60}\text{Te}_{40}$	
Pd-Sn-Te	Kojonenite	$\text{Pd}_{7-x}\text{SnTe}_2$	Isothermal section, 400	Full	Vymazalová and Drábek (2010)
Pd-Te-Se	Miessiite	$\text{Pd}_{11}\text{Te}_2\text{Se}_2$	None		
Rh-Pd-As	Rhodarsenide	$(\text{Rh},\text{Pd})_2\text{As}$	Tentative	Partial, $\text{As-PdAs}_2\text{-RhAs}_2$	Pratt (1994) based on data from Bennett and Heyding (1966)
	Palladodymite	$(\text{Pd},\text{Rh})_2\text{As}$	Isothermal section, 750		
Pt-As-S	Platarsite	PtAsS	Isothermal section, 1000	Full composition	Skinner et al. (1976)
Pt-Bi-Te	Maslovite	PtBiTe	None		
Pt-Cu-Fe	Tulameenite	$\text{PtFe}_{0.5}\text{Cu}_{0.5}$	Isothermal section, 600, 1000	Full composition	Shahmiri et al. (1985)
Pt-Cu-S	Malanite	CuPt_2S_4	None		

Pt-Cu-Sn	Tatyanaite	$\text{Pt}_9\text{Cu}_3\text{Sn}_4$	None			
Pt-Fe-Ni	Ferronickelplatinum	$\text{PtFe}_{0.5}\text{Ni}_{0.5}$	None			
Pt-Hg-Se	Jacutingaite	Pt_2HgSe_3	Isothermal section, 400	Full composition	Drábek et al. (2012)	
Pt-Pd-S	Braggite	(Pt,Pd)S	Isothermal section, 800, 1000	Partial composition; Pd-Pt-PtS- PdS	Cabri et al. (1978)	
			Isothermal section, 1000	Full composition	Skinner et al. (1976)	
Pt-Pd-Sb	Genkinite	$(\text{Pt},\text{Pd})_4\text{Sb}_3$	Isothermal section, 600	Partial composition; $\text{Pd}_{72}\text{Sb}_{28}$ - $\text{Pt}_{84}\text{Sb}_{16}$ -Sb	Kim and Chao (1996)	
			Isothermal section, 800, 1000	Full composition		
			Isothermal section, 1000	Full	Kim (2009)	
Rh-As-Ni	Zaccariniite	RhNiAs	None			
Rh-As-S	Hollingworthite	RhAsS	None			
Rh-Cu-S	Cuprorhodsite	CuRh_2S_4	Isothermal section, 500, 700, 900	Full	Karup-Møller and Makovicky (2007)	
			Isothermal section, 540	Partial, $\text{Cu}_{2-x}\text{S}-\text{Rh}_{17}\text{S}_{15}$ - RhS_3 - $\text{Cu}_x\text{RhS}_{3+x}$ - Cu_{2-x}S		
Rh-Fe-S	Ferrorhodsite	FeRh_2S_4	Isothermal section, 500, 900	Full composition	Makovicky et al. (2002)	
			Vertical section 900–1500	Partial composition; $\text{FeS}_{1.09}$ -FeRh	Bryukvin et al. (1990)	
			Vertical section 1050–1350	Partial composition; $\text{FeS}_{1.09}$ - Rh_2S_3		
			Liquidus projection	Partial composition; $\text{Rh-Rh}_{40}\text{S}_{60}$ - $\text{Fe}_{48}\text{S}_{52}$ -Fe		
Rh-Pb-S	Rhodplumsite	$\text{Rh}_3\text{Pb}_2\text{S}_2$	None			
Ru-As-S	Ruarsite	RuAsS	None			

Pd-As-Sb, Pd-As-Hg, Pd-Cu-Sn, Pt-Cu-Sn, Pt-Bi-Te). We summarize the ternary PGM (taking into the account the ideal composition of minerals) and corresponding systems, and refer to data on phase diagrams in the literature ([Table 10.4](#)). There are still a large number of systems containing PGE-bearing ternary minerals without a knowledge of ternary phase diagrams and phase relations. As shown in [Table 10.4](#), there is still not enough knowledge on several complete isothermal sections and very few systems have been studied at more than one temperature. Furthermore, some ternary systems also require re-investigation due to new observations within the corresponding binary systems and by the discovery of new minerals.

10.2 EXPERIMENTAL METHODS FOR SYNTHESIS OF PLATINUM-GROUP MINERALS

Experimental studies have various implications for geological processes. One of the aims of experimental synthesis is to determine phase relations under specific conditions with a view to understanding natural processes. The knowledge of phase relations allows prediction of the mineral assemblages stable at natural conditions. Experimental study of thermal stabilities and the solid solutions of PGM help to understand their formation, occurrence, and accumulation in nature, thus are directly applicable to the study of mineral deposits.

The other aim of experimental synthesis of PGE compounds is to obtain single crystals of sufficient size for detailed investigations. Single crystals can be studied in terms of crystal structure determination that is also applicable to the mineralogy of PGM. The knowledge of crystal structures and structural mechanisms of various substitutions within PGM also have implications in mineral processing and geo-metallurgy. Various PGE compounds are also of materials science interest and have industrial applications whereby PGE phases are studied in terms of specific properties (e.g., chemical, electrical, optical, magnetic, semiconductor, etc.).

We describe the preparation methods that can be used for PGE phases and minerals synthesis. In the first part ([Section 10.3](#)) we focus on methods resulting in powder products and in the second part ([Section 10.4](#)) we discuss suitable methods for producing single crystals. We also provide some examples of crystal growth and synthesis conditions for various PGE phases and minerals that might be applicable for preparation of other PGE compounds.

10.3 POWDER SAMPLES

10.3.1 DRY TECHNIQUE

The silica-glass tube method belongs to the classical experimental methods, so-called dry technique or solid phase synthesis. The method has been described in detail by [Kullerud \(1971\)](#), focusing on sulfide synthesis.

The silica tube method is suitable for synthesis of PGE sulfides, selenides, and tellurides, as well as for other compounds and alloys that are formed at temperatures below 1300°C (when silica starts to recrystallize and may become permeable). Charges are carefully weighed out from the pure elements

and placed into the silica-glass tube. The starting materials are either pure elements or presynthesized phases, or combinations. To prevent loss of material to the vapor phase during experiments, the free space in the tubes is reduced by placing closely fitting glass rods over the charge. The charges should be as small as possible, but still having the sufficient material for the product investigation (e.g., polished section, X-ray diffraction). Smaller quantities are easier to homogenize, and another consideration is the high prices of pure platinum-group-element starting reagents. The tubes with the charge are evacuated and subsequently sealed in, e.g., a hydrogen-oxygen flame. The capsules with the charge are then heated in horizontal or vertical furnaces, which allow faster quenches. In order to ensure the homogeneity, the samples are after the first melting/heating opened and the products are finely reground under acetone in an agate mortar. In some cases, the reground samples are pelletized under pressure before being reinserted in silica tubes, evacuated and reheated (e.g., Cabri, 1973; Cabri et al., 1976 (palladobismutharsenide)). In many cases the samples are reground several times during the heating before the equilibrium is attained. Reactions in silica tubes rely on diffusion and can be exceedingly slow, particularly for PGE-rich phases and for phase studies at low temperatures. Therefore, some experiments require long term heating to reach the equilibrium that may take from several months up to a year. After heating the experimental runs are quenched by dropping the capsule in cold water.

In order to obtain sulfides with high sulfur content (e.g., PtS_2), a long silica tube located in a temperature gradient (Pt in a hot and S in a cold zone) can be used to prevent the explosion of the tube that might be caused by the high sulfur vapor pressure.

The run products are suitable for powder X-ray diffraction analyses, and are usually examined in polished sections using reflected light microscopy, electron-scanning microscopy and electron-microprobe techniques. In most cases, the run products are very fine grained and required detailed and precise examination (Fig. 10.1A,B).

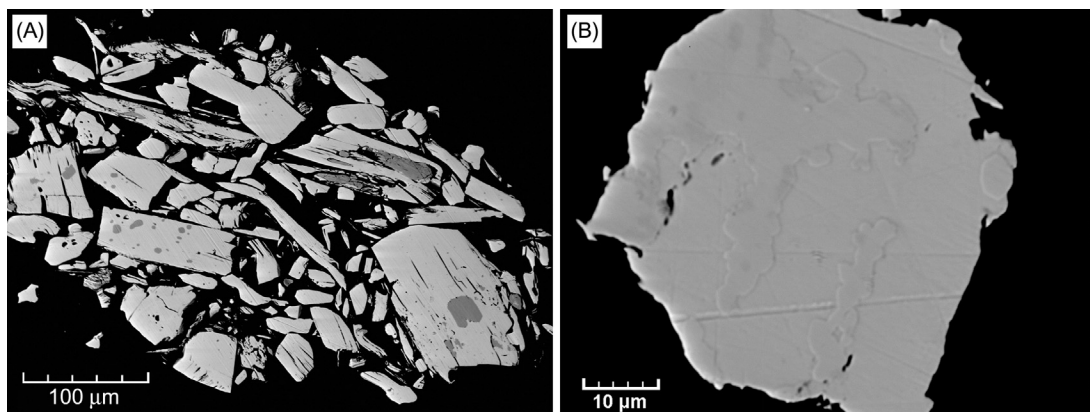


FIGURE 10.1

Back-scattered electron images of experimental products obtained by the dry technique: (A) synthetic jacutingaité (Pt_2HgSe_3) in association with sudovikovite (PtSe_2), a quench from 400°C (heated for 71 days); (B) fine grained intergrowths of lukkulaisvaaraite ($\text{Pd}_{14}\text{Ag}_2\text{Te}_9$) with telargpalite ($\text{Pd}_{2-x}\text{Ag}_{1+x}\text{Te}$) and hessite (Ag_2Te), a quench from 350°C (heated for 130 days).

10.4 SINGLE CRYSTALS

Single crystals of PGE phases and minerals are required for crystal structure investigations and for more accurate determination of their properties. In some cases, phase associations obtained in the form of sufficiently large coexisting crystals help the study of phase relations. Crystal growth techniques can in general be divided into congruent and incongruent. Congruent techniques constitute crystal growth from the melt of the desired substance (melt of a similar composition) and are characterized by a $L \rightarrow S$ phase reaction. Incongruent techniques are based on crystal precipitation from liquid or gas solvents. The principal methods are vapor transport, hydrothermal (water solution) and flux techniques. Moreover, techniques can be distinguished based on spontaneous crystallization (when crystals are formed via nucleation) or controlled crystallization (with seed crystals). The silica-glass tube method (dry technique or so-called solid phase synthesis technique) described in Section 10.3 also allows the preparation of micrometer-size crystals.

10.4.1 CONGRUENT TECHNIQUES

There are various congruent techniques for crystal preparation (e.g., [Wilke, 1973](#)), and all of them are based on a gradual removal of heat from the liquid-solid boundary; they differ in the way this boundary is shifted. An advantage of incongruent techniques is the possibility of synthesizing incongruently melting crystals and synthesis at lower temperatures.

The Bridgman–Stockbarger technique (or Bridgman technique, [Bridgman, 1925](#)) is usually performed in a vertical reaction vessel with a cone-shaped bottom. The vessel with the melt is slowly moved down to the gradient tube furnace, where the temperature in its lower part is lower than in its upper part. Crystallization starts from the bottom of the vessel. The cone shape of the bottom ensures the formation of a single nucleus rather than several. Sometimes a process in which the reaction vessel is cooled in the temperature gradient without moving along the gradient furnace is also called the Bridgman technique.

The Czochralski technique ([Czochralski, 1918](#)) is implemented by gradually pulling the cooled seed crystal above the free surface of the melt. The Kyropoulos technique ([Kyropoulos, 1926](#)) is similar but differs in that there is no mechanical movement of the seed crystal. The temperature of the melt is slowly decreased so that the crystal gradually grows on the seed forming a half-sphere.

Crystal growth via the Verneuil technique is implemented by gradually adding melt droplets to the surface of the growing crystal.

The Pfann technique or zone melting constitutes melting by a movable circular heater of a powder-like starting mixture, which usually is compressed into a cylindrical shape ([Pfann, 1966](#)).

Phases suitable for growing crystals from their melt can be identified from the corresponding known phase diagrams by having a common liquidus and solidus maximum. For example, in the system Pd–Te: the phases Pd_8Te_3 , $PdTe$ (kotulskite) and $PdTe_2$ (merenskyite) display this property. Most of the congruently melting crystals of chalcogenides and pnictogenides are grown using the Bridgman–Stockbarger technique. For example, crystals of $PdTe_2$, up to 7×16 mm in size, were grown using this method by [Lyons et al. \(1976\)](#). The growth was carried out in a silica-glass reaction vessel, which was moved down at 2.8 mm/hour inside a gradient furnace with the temperature of the hot zone at 800°C . Apparently, crystals of other congruently melting phases can be prepared

using a similar technique: PtAs₂ (sperrylite), PdBi (polarite), Pd₃Pb (zvyagintsevite), PdSb (sudburite), Pd₂Si (palladosilicide), PtSb₂ (geversite), Pt₃Sn (rustenburgite), PtSn (niggliite), Rh₂Se₃ (bowieite), PtSe₂ (sudovikovite), PtTe₂ (moncheite), and others.

Congruent techniques are mainly used to grow single phase samples at temperatures near the liquidus and therefore in general are not suitable for studies of phase relations.

10.4.2 INCONGRUENT TECHNIQUES

10.4.2.1 Vapor Transport Technique

In the vapor-transport crystal-growth technique ([Schafer, 1962](#)), a solid substance interacts with a transport agent via a reversible chemical reaction, forming only gas products which flow to another part of the reaction system with different physical and chemical conditions, where the initial substance is formed again but in a single-crystal state. The main requirements for the transport are a concentration gradient and a reversible transport reaction. Usually the transport agents are halogens or their compounds (e.g., ICl₃, AlCl₃, S₂Cl₂). The transport of transition elements (PGE and Fe, Ni, Co) can be facilitated by phosphorus, oxygen, hydrogen and, consequently, water. The vapor transport process is similar to sublimation but it can occur at lower temperatures. To describe the temperature profile of the transport it is convenient to use the $T_1 \rightarrow T_2$ notation where T_1 is the temperature of the charge and T_2 is the temperature of the growth zone.

Crystal growth is usually performed in closed cylindrical reaction vessels made of silica or ordinary glass. A part of the charge (the solid substance) with the transport agent is placed at one end of the vessel. Usually the quantity of the transport agent is orders of magnitude less than that of the charge. In order to create different temperatures at the two ends of the vessel, gradient furnaces or a natural temperature gradient are used. Cylindrical silica ampoules can be used in the vapor transport technique if the hot end of the ampoule is at a temperature not higher than 1000–1200°C. At higher temperatures silica-glass softens, recrystallizes or reacts with a charge, and silica becomes permeable to gas(es). If the hot end of the ampoule has to be at a temperature greater than 1300°C, a white-hot wire is soldered into the ampoule.

[Campbell et al. \(1949\)](#) described transport of various metals including iridium, osmium, platinum, rhodium, and ruthenium using CO and halogens as transport agents. The formation of platinum whiskers by decomposition of platinum chloride at 800°C was described by [Brenner \(1956\)](#). [Schafer \(1962\)](#) results in the formation of iridium (1325→1130°C) and platinum crystals (temperature in the hot end = 1500°C) using oxygen as a transport agent. At similar or lower temperatures, in a flow of oxygen, crystals of PGE oxides such as: OsO₂ ([Rogers et al., 1969; Yen et al., 2004](#)), RuO₂, and IrO₂ ([Rogers et al., 1969; Horkans and Shafer, 1977](#)) or Ru_{1-x}Ir_xO₂ ([Georg et al., 1982](#)) can be also grown. Tiny crystals of osmium phosphide OsP₂ were grown at 1000°C using iodine ([Bugaris et al., 2014](#)) and crystals of palladium arsenides (Pd₃As and Pd₅As) were grown at 500–600°C using chlorine by [Saini et al. \(1964\)](#) who noted that the transport does not occur with other halogens.

Crystals of chalcogenides are usually prepared using halogens. Crystals of RuS₂ and RuSe₂ were prepared following such an approach by, e.g., [Bichsel et al. \(1984\)](#), [Vaterlaus et al. \(1985\)](#), [Fiechter and Kühne \(1987\)](#). The growth of RuS₂ occurred in the temperature profile 1040→1020°C using a mixture of ICl₃ and S₂Cl₂ as transport agents with an excess of sulfur. As a result, crystals

$4 \times 4 \times 4$ mm in size were obtained in about 30 days. The growth of RuSe_2 occurred at $1100 \rightarrow 1070^\circ\text{C}$ using ICl_3 ; the charge also contained an excess of the chalcogen, and as a result $10 \times 8 \times 5$ mm crystals were grown. Crystals of RuTe_2 were grown using ICl_3 at $1060 \rightarrow 960^\circ\text{C}$ over a period of 10 days (Huang et al., 1994) and Colell et al. (1994) synthesized RuS_2 crystals containing up to 50 at.% Ir (temperature profile $1100 \rightarrow 1050^\circ\text{C}$) using iodine. Similarly, Tsay et al. (1994) grew iron-doped RuS_2 crystals using ICl_3 . Crystals of Rh_2S_3 were synthesized within a temperature profile from $1000 \rightarrow 1020^\circ\text{C}$ using bromine (Parthe et al., 1967).

Crystals of PtS_2 were grown using a mixture of chlorine and phosphorus (Finley et al., 1974). The charge contained platinum, sulfur, and phosphorus with molar ratios 1:3:1. Chlorine was added in order to create a pressure of 10,000 Pa. The ideal temperature profile was from $800 \rightarrow 740^\circ\text{C}$, under which flat hexagonal crystals with sizes up to 5×5 mm were grown after 6 days. At lower temperatures ($700 \rightarrow 670^\circ\text{C}$) the transport was insignificant and at higher temperatures ($900 \rightarrow 840^\circ\text{C}$) the two-phase association $\text{PtS} + \text{PtS}_2$ was obtained. Crystals of $\text{Pt}(\text{S},\text{Se})_2$, with varying S/Se ratios, in association with crystals of PtTe_2 , were prepared with phosphorus as the major transport agent, sometimes with addition of chlorine, with temperatures of $850 \rightarrow 875^\circ\text{C}$ at the hot end and $750 \rightarrow 690^\circ\text{C}$ in the cold end (Soled et al., 1975, 1976).

10.4.2.2 Hydrothermal Techniques

Solution and hydrothermal techniques are based on recrystallization of the substance in aqueous solutions at room or higher temperature. At low temperatures, unlike in the vapor transport technique, supersaturation can be reached by gradual evaporation of the water solution; by addition of compounds that lower the solubility of the desired phase (e.g., pH variation); by mixing solutions containing the components of the substance crystallized; electrolysis; transport reactions; and substance exchange on the boundary of two phases. The gradual temperature increase causes an increase in the solubility of most chemical compounds, reaction rates, and diffusion rates. However, the synthesis needs to be done in durable hermetic vessels (autoclaves) at temperatures above 100°C . Usually transport is driven by a temperature gradient and the migration of the phase(s) occur(s) mostly via convection. Often, in order to increase the solubility of the charge, a mineralizer (e.g., KClO_3), which is similar to the transport agent in the vapor transport technique, is added to water. Mineralizers do not form separate phases. The transport of chalcogenides can be increased by adding acid or NH_4I to the water, as chalcogenides decompose in alkali solutions. Iodides (e.g., NH_4I) are the most preferable halogenides because iodine and sulfide ions have the largest difference in ionic radius, which prevents iodine from substituting into the lattice of the growing sulfide.

Most often autoclaves made of stainless steel or titanium alloys are used as laboratory vessels for hydrothermal synthesis, and allow for operating at temperatures up to $\sim 500^\circ\text{C}$ and pressures up to 2000 atmospheres. The solution is often placed in a Teflon or a noble metal liner to protect the autoclave. Hermetic ampoules made of noble metals or silica glass, and of a size less than the internal volume of the autoclave, can be also used to protect from an aggressive environment. Free external space in this case is filled with water. When soft metal ampoules are used, the water often serves as the pressure medium. Ampoules made of noble metals in some cases are the source of the noble metal. When silica ampoules are used, the external water creates a counterpressure that protects the silica ampoule from destruction. Gas, e.g., CO_2 (Rau and Rabenau, 1968) also can be used as the external medium.

Crystals of various metals including platinum were grown hydrothermally by, e.g., [Rau and Rabenau \(1968\)](#). The crystal growth was carried out in silica ampoules in concentrated aqueous solutions of HCl, HBr, or HI in a temperature gradient (with a hot end 420–600°C). To prevent the ampoules from cracking they were placed in autoclaves together with dry carbon dioxide which created the counter-pressure by evaporation. It was also shown that the addition of oxidizers, e.g., Cl₂, Br₂, H₂O₂ or residual oxygen boosts the metal transport due to the increase in concentration of metal ions dissolved in water. [Schwartz et al. \(1982\)](#) prepared platinum oxide crystals (β -PtO₂) in equilibrium with other compounds (e.g., CdPt₃O₆) in sealed platinum ampoules in KClO₃ solution by cooling the solution. Crystals of Rh₂S₃ and Rh₁₇S₁₅ with sizes up to a hundred microns were prepared by, e.g., [Zhang et al. \(2009\)](#), using rhodium carbonyl Rh₆(CO)₁₆ and crystals of sulfur as starting chemicals, grown in Teflon-lined autoclaves at 200–400°C.

The hydrothermal technique is less commonly used to grow PGE-bearing crystals. However, it has been used to study the conditions of formations as in, e.g., the Pd-Sn-Cu-HCl system by [Evstigneeva and Nekrasov \(1980\)](#).

10.4.2.3 Flux Technique

The flux technique (e.g., [Wilke, 1973](#)) is based on the gradual cooling of a multicomponent system. The solubility of the components in the melt decreases with decreasing temperature and this leads to the formation of crystals of certain compounds. Due to the complexity of a multicomponent system the composition of the grown crystals differs from that of the melt. The flux technique is somewhat intermediate between hydrothermal (incongruent) and congruent techniques. The major advantage of the flux technique, in comparison with the hydrothermal technique, is the broad range of temperatures (from 25°C to 1500°C) that can be used for synthesis. The other advantage is the large variety of possible solvents, e.g., various combinations of oxides, salts, hydroxides, and other heteropolar compounds that can be used. Metals with low melting temperature such as Sn, Pb, Bi, Te, In, Hg, eutectic mixtures of lead fluoride or lead oxide, tungsten, molybdenum oxides, or metal halides or alkali metal poly-chalcogenides (e.g., Na₂S_n) are often used as solvents.

In general, the flux method is not very complicated. Specific amounts of the charge and the solvent, in powder form, are placed in a crucible made of inert material. Usually the crucible is tightly closed with a lid to reduce evaporation of the solvent. Then during the shortest possible period of time (several hours) the crucible is heated up to the maximum point. After this, the temperature is quickly decreased by 50–100°C to create a supersaturation or to form nuclei of the desired compound, and then the temperature is slowly decreased at 3–5°C per hour. Afterwards, at a certain temperature the experimental product is quenched or the melt is mechanically separated from the crystals (decanted). In some cases, the crucible with the charge is not quenched or cooled to the room temperature because the desired phase can precipitate as crystals only within a certain temperature interval. In some cases, more complicated cooling modes are used, such as oscillations in the area where crystallization starts. Crucibles used for crystal growth are made most often from precious metals, corundum, or silica-glass tubes. However, as described for dry synthesis in [Section 10.3](#), the silica-glass softens at temperatures over 1300°C and dissolves at temperatures over 600°C in PbF₂-PbO melts.

The flux method is quite universal; crystallization may be possible in poorly concentrated solutions as well as in highly concentrated solutions for a single-component composition, almost in the field of crystallization from the melt. When the solution of a desired material shows a low degree

of concentration then the method displays similarities with the hydrothermal or vapor-transport techniques. In cases where the composition of the solution is almost identical with the crystallized substances then the flux method is similar to synthesis from the melt of the desired compound, like the Bridgman or Czochralski techniques. Usually the term “flux technique” is used when the amount of compound being crystallized is more than 6%–8% of the total liquid phase. However, the self-flux technique can be also distinguished when the composition of an initial melt is the same as that of the resulting crystals. Supersaturation is most commonly created by a slow cooling or by gradual evaporation of the solvent. In some cases, small crystals are obtained under isothermal conditions.

10.4.3 PGE-BEARING CRYSTALS PREPARED BY FLUX TECHNIQUE

The first crystals of PGE compounds using the flux technique were obtained in the 19th century (e.g., [Rossler, 1895](#); as summarized in [Chirvinskii, 1995](#)). For example, dendritic crystals of gold and platinum were prepared by melting Au/Pt with NaCl, $\text{Na}_2\text{S}_2\text{O}_7$ or $\text{Fe}_2(\text{SO}_4)_3$, PtAs₂ (sperrylite), PtSb₂ (geversite) and PtBi₂ (insizwaite) crystals in lead flux, and crystals of RuS₂ (laurite) and PtS₂ by melting Ru (or Pt) in iron sulfide and borax together at $\sim 900^\circ\text{C}$.

Crystals of PGE compounds can be grown in various solvents by gradually decreasing temperature. Reviews by [Fisk and Remeika \(1989\)](#) and [Canfield and Fisk \(1992\)](#) summarize the application of low-temperature melting metals to prepare crystals by the flux method for many chemical compounds including PGE-bearing phases. The growth of UPt₃, NpPt₃, PtMnSb, and UIr₃ crystals in bismuth, RRh₄B₄, RIr₂, and UIr₃ in copper, RPt₂ and YbPt_x in lead, and R₃Rh₄Sn₁₃ in tin (where R is a rare-earth element) was shown by [Fisk and Remeika \(1989\)](#). Further, crystals of UPt₃, YPd, RBiPt, and R₃Bi₄Pt₃ prepared in bismuth; R₂Pt₄Ga₈ in gallium, LaPbPt, CePbPt, LaBiPt, CeBiPt, and PrBiPt in lead, and U₃Sb₄Pt₃ and PtSb₂ in antimony are summarized in [Canfield and Fisk \(1992\)](#). Melts of Al, Ce, Fe, In, Hg, Zn, and Ag can be used to prepare PGE-bearing crystals. Here we provide some examples for crystal growth of PGE-bearing phases and minerals and discuss the experimental conditions.

Crystals of PGE with P, As, Sb, Bi (pnictides) phases can also be prepared by cooling the metal melts. For example, crystals of RhP₃ were grown in tin flux ([Odile et al., 1978](#)); the synthesis was done in silica-glass tubes, where tin formed about 85% of the total volume of the charge. Tubes with the charge were heated to 1150°C for some hours, until complete dissolution. Afterwards, the tube with the charge was cooled to 550°C at a rate of 5°C per hour and the experimental products were washed from tin in hydrochloric acid. Similarly, by cooling the tin melt, other PGE-bearing phosphides can be synthesized, as PtP₂, RuP₂, IrP₂, RuP₄, and OsP₄ ([Baghdadi et al., 1974](#); [Kaner et al., 1977](#) [Ruehl and Jeitschko, 1982](#)), OsP₂ and OsAs₂ or OsSb₂, in an excess of antimony ([Bugaris et al., 2014](#)). [Savilov et al. \(2005\)](#) prepared the ternary phase Pd_{7-x}SnTe₂, an analogue of kojonenite, using a tin flux.

Ternary PGE arsenides can be also synthesized in a metal flux. For example, crystals of BaRh₂As₂ were grown in a lead flux ([Singh et al., 2008](#)) with an initial mixture of Ba_{1.1}Rh₂As_{2.1}Pb₅₀. Due to the presence of barium the synthesis was performed in a glass made of Al₂O₃, sealed in an evacuated silica-glass tube. The mixture was cooled from 1000°C to 500°C at a rate of 5°C per hour. As a result, crystals $1.5 \times 1.5 \times 0.1 \text{ mm}^3$ in size were obtained. The authors did not mention if lead was present in the resulting crystals.

Further, the flux technique can be applied for PGE oxides. For example, needle-like crystals of CaIrO_3 were grown in platinum crucibles with $\text{CaCl}_2 + \text{Ca}(\text{OH})_2 + \text{Ir}$ melt (in molar ratio 10:1:1) by cooling from 827 to 327°C at a cooling rate of 10°C per hour (Sugahara et al., 2008).

The flux method can be also used for crystal growth of PGE chalcogenides. For example, crystals of CuIr_2S_4 were grown by cooling a bismuth-based melt (Matsumoto and Nagata, 2000) from an initial temperature of 1100–1000°C to a final temperature of 500°C. The bismuth melt was decanted and the remaining crystals were washed from the residual bismuth in warm nitric acid. The authors also noted that these crystals could not be prepared by the vapor transport technique and using melts based on Cu, Sn, In, S, and Te. Crystals of RuS_2 (analogue of laurite), RuSe_2 and RuTe_2 in sizes up to 4 mm were grown in bismuth, and tellurium, respectively, using evacuated silica-glass tubes, cooled from 1000°C at a rate of 2°C per hour (Foise et al., 1985). Due to density differences, crystals of Ru chalcogenides grew above the melt. However, crystals grown in bismuth melts may contain some admixture of Bi, up to 3%.

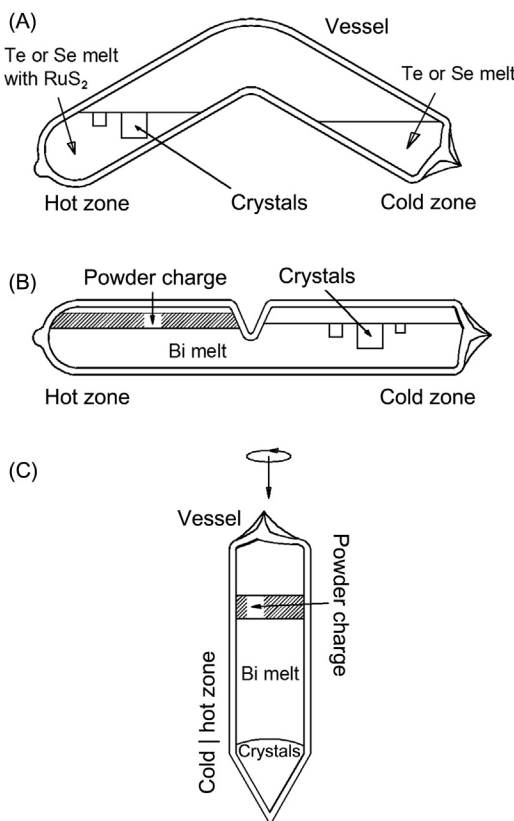
The same approach was also applied by Ezzaouia et al. (1985) to grow crystals of RuS_2 in a tellurium flux by cooling from 1000°C to 850–700°C at rates of 0.7 or 1.4°C per hour. Iridium-rich crystals of RuS_2 (Colell et al., 1994) were prepared from an initial mixture of $\text{Ir}_{0.667}\text{xRu}_{1-\text{x}}\text{S}_2$ with bismuth, in a ratio 1:40, in an evacuated silica-glass tube, heated at 1100°C for a day. Afterwards the experiment was cooled to room temperature at a rate of 2°C per hour, and the crystals were washed in HNO_3 . It should be noted that often solid solutions of Ir-bearing crystals grown by cooling are zoned. Iron-doped RuS_2 crystals (sizes up to 3 mm) were prepared by Tsay et al. (1994) using a tellurium flux (100 g of Te to 5 g of charge) cooling from 1000°C to room temperature at a rate of 1–0.7°C per hour. In order to obtain larger crystals, already-presynthesized crystals can be used as seed material. This approach was used by, e.g., Tsay et al. (1995), following Tsay et al. (1994), to grow crystals of RuS_2 , RuSe_2 , and RuTe_2 reaching sizes of $15 \times 10 \times 10$ mm.

Os chalcogenides can be prepared using methods similar to the one used for Ru chalcogenides (Ezzaouia et al., 1984). Crystals of OsS_2 were grown in sulfur and tellurium and OsSe_2 in tellurium, with ratios of charge to solvent from 1:8 to 1:4 and 1:32 to 1:12, when using tellurium. The silica-glass tube with the charge was heated, in the case of tellurium, at 885°C for 12 hours and cooled to 600°C at a rate of 1°C per hour. For sulfur, the experiment was heated at 650°C and cooled to 300°C at the same rate. The resulting crystals, up to one mm in size, were washed from the tellurium in aqua regia and the sulfur was removed by evaporation (Ezzaouia et al., 1984).

The growth of RuS_2 and OsS_2 crystals using the sulfur flux or RuTe_2 and OsTe_2 using tellurium flux can be considered as a self-flux technique. Applying a similar approach, crystals of Ir_3Te_8 were grown by cooling tellurium flux from 1000°C to 700°C (Liao et al., 1997) and platinum-doped IrTe_2 crystals by cooling from 1160°C to 900°C (Pyon et al., 2013). The chalcogen flux can be applied to crystal growth of those chalcogenides that are in equilibrium with the respective chalcogen. The possibility of preparing only chalcogen-rich substances limits the self-flux technique.

In cases where the solvent has a sufficient partial vapor pressure, then the crystals can be grown by evaporation resulting in crystals of monolayers growing at a constant temperature unlike what occurs during cooling. Zoned crystals are not formed.

The application of evaporation can be nicely demonstrated by the crystal growth of RuS_2 , as documented by Fiechter and Kühne (1987), and earlier by Ezzaouia et al. (1983, 1985). A boomerang-shaped silica-glass tube (by oxygen torch) was used as a reaction vessel (Fig. 10.2A). A tellurium or selenium melt containing RuS_2 was placed in the left end of the vessel (growth

**FIGURE 10.2**

Reaction vessels showing the growth of RuS₂ crystals: (A) in selenium or tellurium flux by solvent evaporation. The solvent evaporates from the solution in the left part and condenses in the right part; (B) in bismuth flux under gradient conditions, with separated growth and dissolving zones; (C) in the traveling-solvent technique.

Adapted from Fiechter, S., Kühne, H.M., 1987. Crystal Growth of RuX₂ (X = S, Se, Te) by chemical vapour transport and high temperature solution growth. *J. Crystal Growth* 83(4), 517–522.

zone) at 920°C; the solvent gradually evaporates and condenses at the right end of the ampoule at 900°C. Crystals of RuS₂ grew up to 3 mm in size in 5 days and small crystals of RuTe₂ (or RuSe₂) were found in the melt. The authors also noted that bismuth is not suitable for this technique due to its low partial vapor pressure. However, they used a bismuth flux under gradient conditions. A sketch of the reaction vessel is shown in Fig. 10.2B. A silica-glass vessel about 14 cm long consists of two parts with a neck located approximately in the middle of the vessel. The neck enables RuS₂ powder to float on the melt in the left part of the vessel and does not get into the right part (the crystallization zone). At the beginning of the experiment the entire vessel was held for a day at 1000°C, then the right part was cooled at a rate 2°C per hour to 500°C. As a result, crystals of RuS₂ were grown with a surface area of up to 15 mm². According to Fiechter and Kühne (1987)

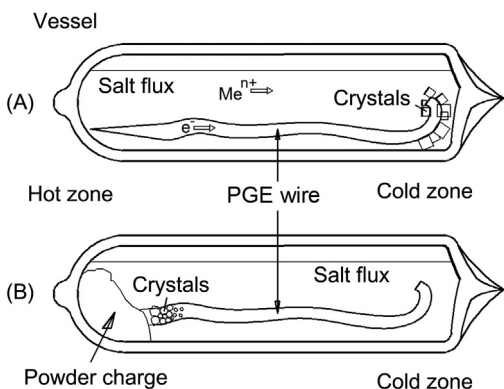
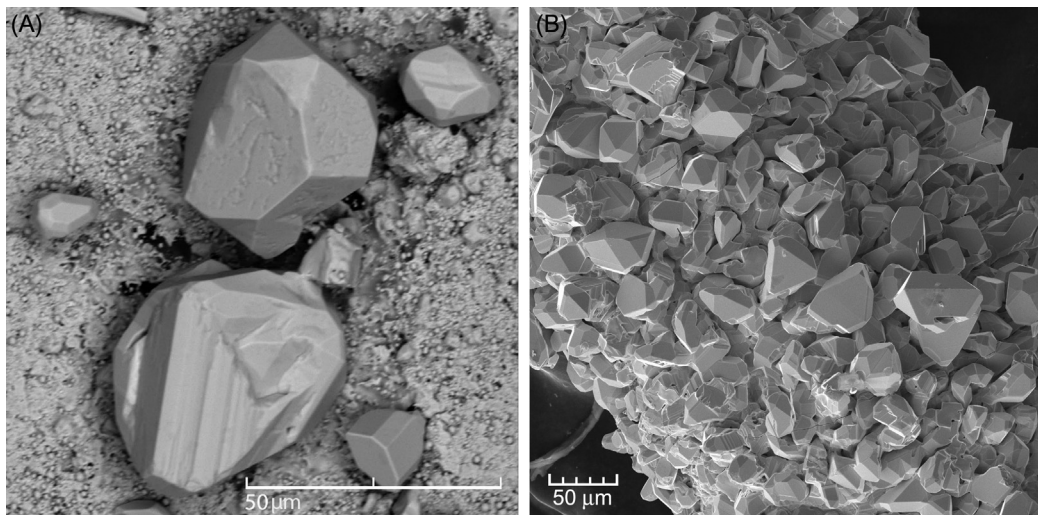


FIGURE 10.3

A reaction vessel for salt-flux synthesis under temperature-gradient conditions for: (A) crystal growth of metals and alloys; (B) crystal growth of Ag-Pd chalcogenides.

this method is the most preferable for Ru chalcogenides. A traveling-solvent technique (Hurle et al., 1967) was applied by Fiechter and Kühne (1987) for RuS_2 crystal growth; a basic outline is shown in Fig. 10.2C. A silica vessel with a conical base (similar to the Bridgeman technique) and a conical tip with a neck on the other end is placed vertically. A hole is made in order that only a single nucleus is formed. In the beginning of the experiment the ampoule contains bismuth melt with RuS_2 powder floating on it. The ampoule is slowly moved down at 0.01 mm/hour into a temperature gradient whereby crystals grow from the base fed by the charge that floats on the bismuth melt.

Gradient conditions can be also applied to obtain some PGE intermetallic phases. For example, crystals (up to 1 mm) of platinum, palladium, and AuPd_4 phase were grown in chlorides of alkali metals (Chareev, 2015). A schematic sketch of the synthesis is shown in Fig. 10.3A. The crystal growth was performed in a salt mixture of $\text{CsCl}/\text{KCl}/\text{NaCl}$, of eutectic composition in silica-glass tubes. A wire made of a noble metal, located along the length of the tube, serves as a source of that metal. The temperature at one end of the tube was about 600°C and in the other end about 50 – 100°C lower. The wire gradually dissolved at the hot end and formed metal crystals on the wire in the cold part of the tube. The metal ions migrate to the place of crystallization via the salt flux and electrons migrate along a wire. Likewise, using an electrically conducting wire it is possible to grow crystals of Ag-Pd chalcogenides (Chareev et al., 2016). The general scheme of the reaction vessel is shown in Fig. 10.3B. The silica-glass tubes were located in a temperature gradient; the hot end was at 450°C , and the cold end about 50°C lower. Material transport occurred in a LiCl/RbCl melt of eutectic composition. A charge of approximate $(\text{Ag},\text{Pd})_4\text{X}$ (where X was S or Se) composition, was placed at the hot end. A wire or a plate of palladium or silver-palladium alloy was touching the charge. After several weeks, small crystals of AgPd_3Se (Fig. 10.4A), in an equilibrium association with $\text{Pd}_3\text{Ag}_2\text{S}$ (coldwellite) and Pd_4S (Fig. 10.4B) were obtained on the wire close to the charge. This technique can be confidently used to grow crystals only of those substances which are in equilibrium with silver-palladium alloy. This ongoing research, focused on

**FIGURE 10.4**

Back-scattered electron images showing: (A) AgPd_3Se crystals with a recrystallized $\text{Pd}_{0.6}\text{Ag}_{0.4}$ plate in the background; (B) equilibrium association of $\text{Pd}_3\text{Ag}_2\text{S}$ (coldwellite) and Pd_4S crystals.

transport of material under gradient conditions, has shown the possibility to grow PtS_2 from $\text{FeS}_2 + \text{Pt}$ charge in the $(850 \rightarrow 780^\circ\text{C})$ profile in eutectic NaCl/KCl .

10.5 PLATINUM-GROUP MINERALS AND SYNTHETIC ANALOGUES

PGM recognized by the Commission on New Minerals, Nomenclature, and Classification (CNMNC) of the International Mineralogical Association (IMA) up to 2002 were summarized and thoroughly evaluated by [Cabri \(2002\)](#). All the pertinent information on the 109 PGM known at that time can be found in this review. An earlier summary of PGM was given by [Cabri \(1981a\)](#). Since 2002 an additional 27 new PGM have been described after approved by CNMNC IMA; in total there are 136 known PGM in 2016. In this chapter, we provide a brief summary of PGM described since Cabri's overview.

All 136 PGM known in 2016 are listed in [Table 10.1](#). The ideal formulae are given as accepted by [Cabri \(2002\)](#); newly described PGM are marked with an *a*. Formulae for atheneite and mertierite II, based on new studies on the crystal structure and formulae of telagpalite and keithconnite, are shown based on the study of the Ag-Pd-Te system by [Vymazalová et al. \(2015\)](#). A summary of PGM data with revised or newly determined crystal structures are presented in [Table 10.2](#). The crystal structures of atheneite, chrisstanleyite, mertierite II, and sopcheite were newly determined, and using synthetic analogues for temagamite and tischendorfite. The crystal structure of atheneite was solved from data collected from a crystal from Itabira, Minais Gerais, Brazil; based on these results ([Table 10.2](#)), the formula was revised to be $\text{Pd}_2[\text{As}_{0.75}\text{Hg}_{0.25}]$ ($Z = 3$) ([Bindi, 2010](#)), instead

of the previously reported $(\text{Pd},\text{Hg})_3\text{As}$ ($Z = 2$) (Clark et al., 1974). The crystal structure of mertierite II was reinvestigated on crystals from the Kaarjolla river, Inari commune, Polar Finland by Karimova et al. (in press), and yielded a formula of that is in agreement with the suggestion of Cabri (2002), proposing the 5:1 ratio for Sb:As. The crystal structure of sopcheite was solved using single-crystal data from the Lukkulaisvaara intrusion, northern Russian Karelia (Table 10.2; Laufek et al., in press). Cooperite (PtS), some of whose phase relations were studied by Cabri et al. (1978), was reinvestigated in terms of crystal structure by Rozhdestvina et al. (2016). They found that in addition to the main reflections (corresponding to the known tetragonal cell, $P4_2/mmc$) there are many weak reflections which fit the tetragonal cell ($I4/mmm$) with double parameters. The crystal structures of isomertieite and törnroosite were refined (Karimova et al., 2016). Table 10.3 summarizes new PGM described after 2002.

As pointed out by Cabri (2002) there is still a significant number of PGM that require re-examination, re-definition or additional data for better characterization, particularly in terms of ideal formula and crystal structure. The main reason for the lack of insufficient identification of PGM is their mode of occurrence (as minute inclusions), intergrowths with other PGM, often embedded in base-metal sulfides and in most cases of very rare occurrence. These peculiarities often prevent XRD-based structural study. Therefore, in some cases further studies of synthetic analogues including crystal structure determination of PGM are desirable, ideally with natural minerals being investigated at the same time. Among newly described PGM (Table 10.3) the synthetic analogues were used in the description of the following mineral species: jacutingaite, milotaita, pašavaite, zaccariniite, lukkulaisvaaraite, kojonenite, palladosilicide, and norilskite. The XRD data were collected and crystal-structure studies were performed on their synthetic analogues, using either single crystals or powder samples. Consequently, the identity of a natural phase can be verified by a synthetic sample. The optical properties, physical properties, and chemical composition must be in agreement. In order to prove the structural identity, various methods can be used. The best way is to compare the X-ray diffraction data of a natural sample with its synthetic analogue (e.g., kitagohaita, sudburyite) but the extraction of a suitable grain of the natural sample is not always possible. Therefore, in order to prove the structural identity of natural and synthetic sample Electron Backscatter Diffraction or Raman spectroscopy (e.g., zaccariniite) can be applied. However, Raman spectroscopy has limited success, particularly among PGE alloy phases. Electron Backscatter Diffraction (EBSD), a technique based on the scanning electron microscope, enables sample microstructure to be analyzed, visualized, and quantified; it is a non-destructive method for the study of tiny grains, *in situ* (*in polished sections*). The diffraction pattern is characteristic of the crystal structure and orientation in the spot where it was generated. Hence the diffraction pattern can be used to determine the crystal orientation, discriminate between crystallographically different phases, characterize grain boundaries, and provide information about the local crystalline perfection. EBSD was used for the description of jacutingaite, pašavaite, lukkulaisvaaraite, kojonenite, palladosilicide, and norilskite. The EBSD technique can be applied as a supporting tool in order to distinguish various PGM minerals with defined crystal structures, but does not work in every case, depending on the polished characteristics of different minerals.

We tabulate all known PGM in 2016 (Table 10.1) and provide a brief overview on new PGM described from 2002 to 2016, as summarized in Table 10.3. Minerals are listed in alphabetical order; the data were collected from the original sources. All listed minerals were approved by the CNMNC of IMA and resulted in a publication except for ferhodsite (IMA No

2009-056, Begizov). The mineral was accepted by the Commission in 2009 but the description has not yet been published so that insufficient information about the mineral composition and other properties is known. Reflectance data for all listed minerals were measured in the range of λ from 400 to 700 nm (in case of pašavaite and jacutingaite from λ 420 to 700 nm). Herein we present only four wavelengths recommended by COM. The strongest lines from the XRD patterns are given, with a reference to the PDF or ICSD databases, if known. An average of electron-microprobe analyses (EMPA) is given for chemical composition. The experimental aspects for the corresponding compound are discussed for each mineral/synthetic analogue. Minerals marathonite $Pd_{25}Ge_9$ (IMA No 2016-080), palladogermanide Pd_2Ge (IMA No 2016-086), kravtsovite $PdAg_2S$ (IMA No 2016-092) and vymazalováite $Pd_3Bi_2S_2$ (IMA No 2016-105) were accepted when this Chapter was completed therefore a detailed description of these four minerals is not provided.

10.5.1 BORTNIKOVITE Pd_4Cu_3Zn

Crystallography: tetragonal, $P4/mmm$?

Unit cell: a 6.00, c 8.50 Å, V 306.0 Å³, Z = 3

X-ray powder diffraction pattern, strongest lines [d in Å(I)(hkl)]: 3.00(1)(200,112), 2.64(1)(120), 2.36(0.5)(113), 2.13(10)(004, 220), 1.737(1)(132), 1.501(3)(400,224), 1.346(2)(240,332), 1.224(8)(404), 1.161(1)(151), 1.059(4)(440), ICDD PDF2 card 00-060-0492

Structure: not defined

Appearance: Forms rims (50–60 µm thick and 50–150 µm long) on isoferroplatinum, inter-growing with titanite and chlorite. Found in a heavy concentrate sample from sediments of the Konder valley.

Optical properties: White with a slight greyish tint in reflected light; bireflectance, anisotropy, and internal reflections not observed.

Reflectance, [\lambda nm, R %]	470	56.9
	546	61.7
	589	63.4
	650	65.4

Physical Properties: Opaque, metallic luster, steel-white with slight cream tint, poorly malleable

Hardness: VHN₂₅ 367.9 (354–382) kg/mm² Mohs

Cleavage: not observed

Density: 11.16 g/cm³ (calc.)

Chemical Composition (EMPA data, wt.%):

Pd 58.19, Pt 4.06, Fe 1.41, Cu 27.26, Zn 8.02 $\sum 98.94(Pd_{3.82}Pt_{0.14})\sum 3.96Cu_{3.00}(Zn_{0.86}Fe_{0.18})\sum 1.04$ ($n=10$)

Pd 62.44, Cu 27.97, Zn 9.59 $\sum 100.00 Pd_4Cu_3Zn$ —ideal

Type locality and occurrence: The Konder placer deposit, Ayan-Maya district, Khabarovsky krai, Russia.

Name: For Nikolai S. Bortnikov of the Institute of Geology of Ore Deposits, Petrography, Mineralogy and Geochemistry RAS, in recognition of his contributions to mineralogy and mineral deposits.

Reference: Mochalov et al. (2007), IMA No 2006-027

Note: Further investigations on XRD data and crystal structure is desirable.

Experimental: The phase diagram of the Pd-Cu-Zn system at 400°C and 800°C was assessed tentatively by Lebrun et al. (2007), based on data of Dobersek and Kosovinc (1989). The corresponding synthetic phase is not known. A further, more detailed experimental study is needed.

10.5.2 COLDWELLITE $\text{Pd}_3\text{Ag}_2\text{S}$

Crystallography: Cubic, $P4_332$

Unit cell: $a = 7.2470 \text{ \AA}$, $V = 380.61 \text{ \AA}^3$, $Z = 4$

X-ray powder diffraction pattern, strongest lines [d in \AA (I)(hkl)]: 2.427(100)(221), 2.302(38)(310), 2.195(38)(311), 1.4280(44)(510,431), 0.9294(24)(650,643), 0.9208(20)(732,651)

Structure: isostructural with β -Mn

Appearance: Discovered in a high-grade heavy-mineral concentrate from the Marathon deposit. Coldwellite (in size $150 \times 80 \mu\text{m}$), is anhedral, slightly angular with scalloped grain edges with overgrowth of vysotskite (PdS); most coldwellite occur in small grains, sizes 0.5–11 μm .

Optical properties: In reflected light white with a light pinkish brown tint, isotropic.

Reflectance [λ nm, R%]	470	41.9
	546	44.9
	589	44.0
	650	45.0

Physical Properties: Opaque, with a metallic luster

Hardness: not measured

Cleavage: not observed

Density: 9.90 g/cm³ (calc.)

Chemical Composition (EMPA data, wt.%):

Pd 56.10 Fe 0.16 Ag 38.20 S 5.63 $\sum 100.09$, $(\text{Pd}_{2.99}\text{Fe}_{0.02})_{\sum 3.01}\text{Ag}_{2.00}\text{S}_{0.99}$ ($n = 23$)

Pd 56.30 Ag 38.05 S 5.65 $\sum 100.00$, $\text{Pd}_3\text{Ag}_2\text{S}$ —ideal

Type locality and occurrence: The Marathon Cu-PGE-Au deposit, Coldwell Complex, Ontario, Canada (48°48'7" N, 86°18'55" W). It was also reported from the PGE-Cr zone of the Birch Lake Deposit, Duluth Complex, Canada (Severson and Hauck, 2003) and in PGE mineralization of the Fedorova-Pana ore node (Subbotin et al., 2012).

Name: After the locality at the Coldwell Complex, Ontario, Canada.

Reference: McDonald et al. (2015), IMA No 2014-045

Experimental: The synthetic analogue occurs as a distinct phase in the ternary system Pd-Ag-S at 400°C and 550°C (Vymazalová et al., in prep.). Based on the experimental study ($\text{Ag}_2\text{S}-\text{Pd}$) of Raub (1954) the phase $\text{Pd}_3\text{Ag}_2\text{S}$ is stable up to 940°C.

10.5.3 FERHODSITE $(\text{Fe}, \text{Rh}, \text{Ni}, \text{Ir}, \text{Cu}, \text{Pt})_9\text{S}_8$

Crystallography: Tetragonal

Unit cell: $a = 10.009$, $c = 9.840$ Å, $V = 985.77$ Å³

X-ray powder diffraction pattern, strongest lines [d in Å(I)(hkl)]: 5.72(50), 3.01(70), 2.81(30), 2.23(100), 1.933(60), 1.772(40), 1.367(3), 1.167(4)

Type locality and occurrence: Nizhny Tagil ultramafic complex, Solovyeva Gora, Alexandrov Log (57°40' N, 59°39' W) and the Konder placer, Konder alkaline-ultrabasic massif, Maya river basin, South Yakutia, Russia (57°36' N, 134°37' W).

Name: For the main chemical components (Fe, Rh, S).

Reference: Begizov V.D., IMA No 2009-056

Note: Approved by IMA in 2009 but no other data on the mineral have been published to date.

10.5.4 JACUTINGAITE Pt_2HgSe_3

Crystallography: trigonal, $P\bar{3}m1$

Unit cell: $a = 7.3477$, $c = 5.2955$ Å, $V = 247.59$ Å³, $Z = 2$

X-ray powder diffraction pattern, strongest lines [d in Å(I)(hkl)]: 5.2917(100)(001), 2.7273(16) (201), 2.4443(10)(012), 2.0349(18)(022), 1.7653(37)(003), 1.3240(11)(004) 1.0449(11)(025)

Structure: The crystal structure was solved and refined from the powder X-ray-diffraction data on synthetic Pt_2HgSe_3 . Isostructural with $\text{Pt}_4\text{Ti}_2\text{X}_6$ ($\text{X} = \text{S}$, Se, or Te); no structural analogue is known as a mineral.

Appearance: Occurs as a single grain (about 50 µm across) in an aggregate (2 mm across) of atheneite, potarite, and hematite, obtained from a heavy-mineral concentrate.

Optical properties: Light gray in reflected light, bireflectance moderate to distinct, a bluish gray to rusty brown pleochroism; anisotropy weak to distinct.

Reflectance [λ nm, R ₁ , R ₂ %]	470	47.4	51.1
	546	48.2	50.5
	589	48.0	49.6
	650	47.1	47.8

Physical Properties: Opaque, gray with a metallic luster and gray streak, brittle.

Hardness: $\text{VHN}_{10} = 169$ (119–245) g/mm², Mohs 3½

Cleavage: {001} very good

Density: 10.35 g/cm³ (calc.), 10.9 (meas. on synth.)

Chemical Composition (EMPA data, wt.%):

Pt 37.30, Pd 5.91, Hg 25.72, Ag 0.16, Cu 0.82 Se 31.48 $\sum 101.39$ ($\text{Pt}_{1.46}\text{Pd}_{0.42}\text{Cu}_{0.10}$ $\text{Ag}_{0.01}\sum_{1.99}\text{Hg}_{0.98}\text{Se}_{3.04}$ ($n = 3$))

Pt 46.73, Hg 24.06, Se 28.33 $\sum 99.12$ ($\text{Pt}_{1.97}\text{Hg}_{1.04}\text{Se}_{2.99}$) (synth., $n = 7$)

Pt 47.14, Hg 24.24, Se 28.62 $\sum 100.00$ Pt_2HgSe_3 —ideal

Type locality and occurrence: The Cauê iron-ore deposit, Itabira district, Minas Gerais, Brazil

Name: After the specular hematite-rich vein-type gold mineralization, locally known as “jacutinga,” in which the mineral occurs.

Reference: Vymazalová et al. (2012a), IMA No 2100-078

Note: The structural identity of natural and synthetic Pt_2HgSe_3 was confirmed by electron back-scattering diffraction (EBSD).

Experimental: Phase relations in the system Pd-Hg-Se were studied at 400°C (Drábek et al., 2012). Only one ternary phase (jacutingaite) is known in the ternary system. Jacutingaite forms stable assemblages with tiemannite (HgSe) and sudovikovite (PtSe_2), sudovikovite and luberoite (Pt_5Se_4), luberoite and platinum, and coexists with PtHg , PtHg_2 , PtHg_4 phases. Below 250°C, the phase HgPt is no longer stable and the assemblage $\text{Pt}_2\text{HgSe}_3 + \text{PtHg}_2 + (\text{PtHg})_{ss}$ appears in the system.

10.5.5 JAGUÉITE $\text{Cu}_2\text{Pd}_3\text{Se}_4$

Crystallography: monoclinic, $P2_1/c$

Unit cell: a 5.6719, b 9.9095, c 6.2636 Å, β 115.403°, V 318.0 Å³, $Z = 2$

X-ray powder diffraction pattern, strongest lines [d in Å(I)(hkl)]: 2.759(23), 2.676(100)(121), 2.630(64)(1̄22), 2.508(31)(2̄02), 2.269(27)(041), 1.950(27)(122), 1.920(36)(1̄23), 1.866(24)(2̄41), ICDD PDF2 card -00-057-0615

Structure: Structure solved from a single crystal by Topa et al. (2006), isostructural with chrisstanleyite.

Appearance: Occurs in lobate aggregates with chrisstanleyite (up to 500 µm in across) embedded in calcite or as inclusions of anhedral grains (up to 50 µm across) in tiemannite and naumannite with common twinning.

Optical properties: Light creamy-yellowish in reflected light, bireflectance weak to moderate, pleochroic from a light buff to a creamy buff, strong anisotropy (rotation tints from brownish to bluish, greenish).

Reflectance, [\lambda nm, R ₁ , R ₂ %]	470	air 41.0 50.1	im 27.0 31.9
	546	44.1 51.8	29.2 33.8
	589	44.6 51.7	29.4 33.7
	650	45.1 52.0	30.2 34.1

Physical Properties: Opaque with a metallic luster and black streak, brittle, uneven fracture.

Hardness: VHN_{25} 612 (464–772) g/mm², Mohs 5

Cleavage: not observed

Density: 8.02 g/cm³ (calc.)

Chemical Composition (EMPA data, wt.%):

Cu 15.7, Ag 1.59 Pd 42.04, Se 40.15 \sum 99.48 ($\text{Cu}_{1.91}\text{Ag}_{0.11}\text{Pd}_{3.05}\text{Se}_{3.93}$ ($n = 8$))

Cu 16.68, Pd 41.88, Se 41.44 \sum 100.00 $\text{Cu}_2\text{Pd}_3\text{Se}_4$ —ideal

Type locality and occurrence: Selenide mineralization at El Chire, the depression of Jagué La Rioja province, Argentina (28°38.3' S, 68°44.3' W). Observed, as an unnamed phase, from the Copper Hills occurrence, East Pilbara region, Western Australia (Nickel, 2002).

Name: After the village of Jagué, the closest settlement to the El Chire mine, La Rioja, Argentina.

Reference: Paar et al. (2004), Topa et al. (2006), IMA No 2002-60

Experimental: The synthetic analogue occurs as a distinct phase in the ternary system Pd-Cu-Se at 300 and 400 °C (Makovicky and Karup-Møller, in press).

10.5.6 KALUNGAITE PDASSE

Crystallography: Cubic, $P\bar{a}3$

Unit cell: a 6.089 Å, V 225.78 Å³, Z = 4

X-ray powder diffraction pattern, strongest lines [d in Å(I)(hkl)]: 3.027(75)(002), 1.838(100) (113), 1.172(95)(115,333), 1.077(80)(044,144,334), 0.988(70)(116,235,253), 0.929(90)(335), 0.918 (70)(226), ICDD PDF2 card 00-058-0509

Structure: not defined

Appearance: Occurs as 0.1–0.5 mm platy anhedral aggregates, in association with gold, chalcopyrite, bohdanowiczite, clausthalite, guanajuatite, Pb-Bi-Se-S phase, padmaite, sperrylite, stilbiopalladinite.

Optical properties: In reflected light cream, creamy gray against gold, isotropic, no internal reflections.

Reflectance, [\mathbf{\lambda}nm, R %]	470	air 47.5	im 33.3
	546	46.9	32.6
	589	46.8	32.6
	650	48.0	34.0

Physical Properties: Lead gray with metallic luster, black streak, brittle with an uneven fracture

Hardness: VHN₂₅ 438 (429-455) g/mm², Mohs

Cleavage: not observed

Density: 7.59 g/cm³ (calc.)

Chemical Composition (EMPA data, wt.%):

Pd 41.32, As 27.49, Bi 0.35, Sb 1.59, Se 27.67, S 1.22 \sum 99.64 Pd_{1.01}(As_{0.95}Sb_{0.03}Bi_{0.004})_{0.98}(Se_{0.91}S_{0.10})_{1.01} ($n=8$)

Pd 40.88, As 28.78, Se 30.34 \sum 100.0 PdAsSe—ideal

Type locality and occurrence: The Buraco do Ouro gold mine, Cavalcante town, Goiás State, Brazil (13°47'45" S, 47°27'35" W).

Name: For the Kalunga people, a community of descendants of African slaves living in the surroundings of the mine, Goiás State, Brazil.

Reference: Botelho et al. (2006), IMA No 2004-047

Note: The XRD data of natural sample are in an agreement with the data of the synthetic phase (ICDD PDF2—01-070-8016 card) and would be worth reinvestigation in terms of refinement based on the structural model proposed by Foecker and Jeitschko (2001).

Experimental: The ternary system Pd-As-Se has not been investigated. Nevertheless, the synthetic analogue was studied by Foecker and Jeitschko (2001). They refined the crystal structure of the synthetic PdAsSe from the single crystal XRD data. The phase is cubic, space group $P2_13$, a 6.095 Å, V 226.40 Å³, Z 4, and belongs to the ullmannite (NiSbS) type structure.

10.5.7 KINGSTONITE RH_3S_4

Crystallography: monoclinic, $C2/m$

Unit cell: a 10.4616, b 10.7527, c 6.2648 Å, β 109.000°, V 666.34 Å³, Z = 6

X-ray powder diffraction pattern, [d in Å(I)(hkl)]: 3.156(100)(310), 3.081(100)($\bar{1}31$), 2.957(90)(002), 2.234(60)(202), 1.941(50)($\bar{2}23$), 1.871(80)($\bar{4}41$), 1.791(90)(060, $\bar{1}33$)

Structure: Structure solved and refined from single crystal. A new structure type.

Appearance: Occurs as subhedral (tabular, elongate) to anhedral inclusions (10–40 µm) in Pt-Fe alloy with isoferroplatinum, tetraferroplatinum, Cu-bearing Pt-Fe alloy, osmium, enriched oxide remnants of osmium, laurite, bowieite, ferrorhodsite, cuprorhodsite.

Optical properties: In reflected light pale slightly brownish gray, weakly pleochroic, weak bireflectance, weak to moderate anisotropy (rotation tints in dull grays and browns).

Reflectance, [\lambda nm, R₁, R₂ %]: 470 air 47.2 48.9 im 33.2 34.7,

546 48.4 50.3 34.3 36.1

589 49.1 50.7 35.0 36.5

650 49.8 51.0 35.6 36.7

Physical Properties: Opaque with a metallic luster and black streak, brittle.

Hardness: VHN₂₅ 895 (871–920) g/mm², Mohs 6

Cleavage: good, parallel to [001]

Density: 7.52 g/cm³ (calc.)

Chemical Composition (EMPA data, wt.%):

Rh 46.5, Ir 16.4, Pt 11.2, S 25.6 \sum 99.7 (Rh_{2.27}Ir_{0.43}Pt_{0.29}) \sum 2.99 S_{4.01} (n = 20)

Rh 70.65, S 29.35, \sum 100.00 Rh₃S₄—ideal

Type locality and occurrence: The Bir Bir river, Wallaga province, Yubdo district, Ethiopia. Also observed as inclusions in heavy-concentrate platinum from diamond placers of the Mayat-Vodorazdel'nyi site in the Anabar river basin, Russia (Airiyants et al., 2014).

Name: For Gordon A. Kingston (b. 1939), in recognition of his contributions to PGE mineralogy and geology of related deposits.

Reference: Stanley et al. (2005), IMA No 1993-46

Experimental: The mineral has a synthetic analogue Rh₃S₄ (Beck and Hilbert, 2000; ICSD No 410813, ICDD PDF2 01-070-5129), stable up to 1130°C. The binary system Rh-S comprises another three binary phases Rh₁₇S₁₅, Rh₂S₃ and RhS_{~3} (Predel, 1998). Based on the study of the ternary system Cu-Rh-S by Karup-Møller and Makovicky (2007), the phase Rh₃S₄ dissolves up to 0.6 Cu and 2.8 at.% Cu at 900°C and 700°C, respectively and is not stable at 540°C. The natural mineral may be stabilized by the content of Pt or Ir at lower temperature.

10.5.8 KITAGOHAITE PT₇CU

Crystallography: Cubic, $Fm\bar{3}m$

Unit cell: a 7.7891 Å, V 472.57 Å³, Z = 4.

X-ray powder diffraction pattern, strongest lines [d in Å(I)(hkl)]: 2.246(100)(222), 1.948(8)(004), 1.377(77)(044), 1.174(27)(622), 1.123(31)(444), 0.893(13)(662)

Structure: Ca₇Ge type. The XRD data of kitagohaite were refined by the Rietveld method based on the structural model of a synthetic analogue ([Schneider and Esch, 1944](#); [Sluiter et al., 2006](#)) (ICSD No 108775, ICDD PDF2 01-074-6150 card).

Appearance: The mineral comes from a heavy-mineral concentrate. It occurs in grains (around 0.5 mm in size), rimmed by hongshiite (PtCu).

Optical properties: In reflected light, white, isotropic.

Reflectance [λnm, R%]	470	63.2
	546	66.6
	589	68.2
	650	70.1

Physical Properties: Opaque, greyish white, with a metallic luster and gray streak, malleable.

Hardness: VHN₁₀₀ 217 (206-237) g/mm², Mohs 3½

Cleavage: not observed

Density: 19.958 g/cm³ (calc.)

Chemical Composition (EMPA data, wt.%):

Pt 95.49, Cu 4.78 \sum 100.26 Pt_{6.93}Cu_{1.07} (*n* = 13)

Pt 95.55, Cu 4.45 \sum 100.00 Pt₇Cu—ideal

Type locality and occurrence: The Lubero region of North Kivu, Democratic Republic of the Congo.

Name: For the Kitagoha river, the platiniferous river in the Lubero region, Congo.

Reference: [Cabral et al. \(2014\)](#), IMA No 2013-114

Experimental: It has a synthetic analogue CuPt₇ ([Schneider and Esch, 1944](#)), with an ordered structure whereas above 500°C it becomes disordered, lacking superlattice reflections.

10.5.9 KOJONENITE PD_{7-x}SNTE₂ (0.3 ≤ *X* ≤ 0.8)

Crystallography: tetragonal, *I*4/*mmm*

Unit cell: *a* 4.001, *c* 20.929 Å, *V* 335.0 Å³, *Z* = 2

X-ray powder diffraction pattern, strongest lines [*d* in Å(I)(*hkl*)]: 10.465(29)(002), 2.496(52) (114), 2.1986(100)(116), 2.0930(18)(0010) 2.0025(48)(200), synth. (ICSD PDF2 cards 01-073-5652 and PDF 01-073-9276)

Structure: Structure solved on a synthetic single crystal by [Savilov et al. \(2005\)](#), and confirmed by x-ray powder diffraction data on experimental products ([Vymazalová and Drábek, 2010](#)). Isotypic to nickel analogues of Ni_{7-x}SnQ₂ (Q = S, Se, Te) ([Baranov et al., 2003, 2004](#)), consists of Cu₃Au-like Sn/Pd blocks and NaCl-like Pd/Te slabs.

Appearance: It forms anhedral grains (< 40 µm) in aggregates (up to 100 µm) with kotulskite as inclusions in chalcopyrite and cubanite.

Optical properties: In reflected light slightly pinkish off-white against (kotulskite bright cream), weak bireflectance (visible only on differently oriented adjacent grains), no pleochroism, anisotropy distinct (with rotation tints in shades of dark greenish-brown).

<i>Reflectance, [λnm, R_o, R_e %]</i>	470	nat. 55.0	52.7	synth. 54.8	53.4
	546	58.5	56.5	58.6	56.9
	589	61.0	58.3	61.2	59.4
	650	63.9	60.1	63.8	61.4

Physical Properties: Opaque, metallic luster, brittle, black streak (synth.).

Hardness: not measured

Cleavage: not observed

Density: 10.07 g/cm³ (calc.)

Chemical Composition (EMPA data, wt.%):

Pd 62.48, Sn 11.74, Te 25.63 \sum 99.85 Pd_{5.96}Sn_{1.00}Te_{2.04} ($n = 20$), Pd 63.1, Sn 11.7, Te 25.2—simplified formula for natural sample Pd₆SnTe₂.

Pd 63.8 Sn 11.5 Te 24.7 \sum 100.0 for $x = 0.8$; Pd 65.6 Sn 10.9 Te 23.5 \sum 100.0 for $x = 0.3$

Pd_{7-x}SnTe₂—ideal based on crystal structure of synthetic material.

Type locality and occurrence: the Stillwater Layered Igneous Intrusion, Stillwater Valley, Montana, USA (45°23'11" N, 109°53'03" W). The mineral is known also to occur in Noril'sk ores (Sluzhenikin et al., pers. comm.).

Name: For Kari K. Kojonen (b. 1949) of the Geological Survey of Finland, for his contributions to ore mineralogy.

Reference: [Stanley and Vymazalová \(2015\)](#), IMA No 2013-132

Note: The structural identity between natural and synthetic kojonenite was confirmed by electron backscatter diffraction (EBSD).

Experimental: Phase relations in the system Pd-Sn-Te were determined at 400°C (Vymazalová and Drábek, 2010). At 400°C the system contains three ternary compounds: kojonenite, and phase Pd₇₂Sn₁₆Te₁₂ and PdSnTe, not known to occur in nature. Kojonenite forms a stable assemblage with paolovite (Pd₂Sn, dissolving up to 4 at.% Te) and the ternary phase Pd₇₂Sn₁₆Te₁₂. It also coexists with palladium tellurides kotulskite (PdTe), phase Pd₃Te₂, telluropalladinite (Pd₉Te₄), and keithconnite (dissolving up to 4 at.% Sn). The upper stability of kojonenite is 596°C where it melts incongruently.

10.5.10 LISIGUANGITE CUPTBIS₃

Crystallography: Orthorhombic, $P2_12_12_1$

Unit cell: $a = 7.7152$, $b = 12.838$, $c = 4.9248$ Å, $V = 487.80$ Å³, $Z = 4$

X-ray powder diffraction pattern, strongest lines [d in Å(I)(hkl)]: 6.40(30)(020), 3.24(80)(031), 3.03(100)(201), 2.27(40)(051), 2.14(50)(250), 1.865(60)(232)

Structure: The crystal structure was solved from a single crystal fragment. Belongs to the lapieite group, Pt-analogue of mückeite (CuNiBiS₃) and malyshevite (PdCuBiS₃).

Appearance: Occurs as idiomorphic crystals, generally tabular or lamellae {010}, elongated along [100], up to 2 mm long and 0.5 mm wide. Sampled from a heavy mineral concentrate.

Optical properties: In reflected light, bright white with a yellowish tint, anisotropy weak to moderate (blue-greenish to brownish colors and parallel-axial extinction), no internal reflection, parallel extinction.

<i>Reflectance, [λnm, R₁ R₂ %]</i>	470	air 39.2 36.7	im 23.4 22.3
	546	40.3 37.3	23.6 22.6
	589	40.7 37.9	23.6 22.7
	650	40.8 37.9	23.7 22.9

Physical Properties: Opaque, lead-gray with black streak and metallic luster, brittle

Hardness: VHN₂₅ 48.3 (46.7–49.8) g/mm², Mohs 2½

Cleavage: {010} perfect, {001} distinct, {100} visible

Density: 7.42 g/cm³ (calc.)

Chemical Composition (EMPA data, wt.%):

Cu 12.98, Pt 30.04, Pd 2.69, Bi 37.65, S 17.55 \sum 100.91 Cu_{1.10}(Pt_{0.83}Pd_{0.14}) \sum 0.97 Bi_{0.97}S_{2.96} (*n* = 8)

Cu 11.27, Pt 34.60, Bi 37.07, S 17.06 \sum 100.00 CuPtBiS₃—ideal

Type locality and occurrence: Mineral discovered in a PGE-bearing Co-Cu sulfide vein in garnet pyroxenite of the Yanshan Mountains, Chengde Prefecture, Hebei Province, China. The mineral also observed in Cu-Ni-PGE ores in the footwall of the Sudbury Igneous Complex, Canada (Pentek et al., 2013).

Name: After Li Siguang on the 120th anniversary of his birth (1889–1971); prominent Chinese geologist, a founder of geomechanics, advocate of the theory of tectonic systems, one of the pioneers in oil exploration in China.

Reference: Yu et al. (2009), IMA No 2007-003

Experimental: The quaternary system Cu-Pt-Bi-S has not been experimentally studied. The preliminary experimental results of ongoing research confirm the existence of a synthetic analogue stable at 400°C.

10.5.11 LUKKULAIISVAARAITE PD₁₄AG₂TE₉

Crystallography: tetragonal, *I4/m*

Unit cell: *a* 8.9599, *c* 11.822 Å, *V* 949.1 Å³, *Z* = 2.

X-ray powder diffraction pattern, strongest lines [*d* in Å(I)(*hkl*)]: 2.8323(58)(130,310), 2.8088(92)(213), 2.5542(66)(312), 2.4312(41)(321,231), 2.1367(57)(411,141), 2.1015(52)(233,323), 2.0449(100)(314), 2.0031(63)(420,240), 1.9700(30)(006), 1.4049(30)(246,426), 1.3187(36)(543,453) (synth.).

Structure: The crystal structure was solved and refined from the powder X-ray-diffraction data of synthetic Pd₁₄Ag₂Te₉. Unique structure type; shows some similarities to that of sopcheite (Ag₄Pd₃Te₄) and palladseite (Pd₁₇Se₁₅).

Appearance: Occurs as anhedral grains (about 40 µm in diameter) rimmed by tulameenite and randomly accompanied by telargpalite and Bi-rich kotulskite, enclosed in chalcopyrite, in association with millerite, bornite and hematite. It also is observed as tiny grains (5–10 µm) in intergrowths with telargpalite and Bi-rich kotulskite in association with moncheite, tulameenite, hongshiite, and telluropalladinite.

Optical properties: In reflected light, light gray with a brownish tinge, strong bireflectance, light brownish gray to greyish brown pleochroism, distinct to strong anisotropy; exhibits no internal reflections.

Reflectance, [\lambda nm, R ₁ R ₂ %]	470	40.9	48.3
	546	47.6	56.4
	589	52.1	61.0
	650	57.5	65.2

Physical Properties: Opaque, gray, with metallic luster, and gray streak, brittle.

Hardness: VHN₂₀ 355 (339–371) kg/mm², Mohs 4

Cleavage: not observed

Density: 9.993 g/cm³ (calc.), 9.9 g/cm³ (meas. on synth.)

Chemical Composition (EMPA data, wt.%):

Pd 52.17, Ag 7.03, Te 40.36 \sum 99.56 Pd_{14.05}Ag_{1.88}Te_{9.06} ($n = 5$)

Pd 52.13, Ag 7.31, Te 40.58 \sum 100.02 Pd_{13.99}Ag_{1.93}Te_{9.08} (synth. $n = 9$)

Pd 52.20, Ag 7.56, Te 40.24 \sum 100.00 Pd₁₄Ag₂Te₉—ideal

Type locality and occurrence: The Lukkulaisvaara intrusion, northern Russian Karelia, Russia. (66°19'20" N, 30°49'50" E). Also observed, as an unnamed phase, in the South Sopcha massif and from the Monchetundra deposit of the Monchegorsk Complex, Kola Peninsula, Russia ([Grokhovskaya et al., 2003, 2009](#)).

Name: For the Lukkulaisvaara intrusion in Russian Karelia.

Reference: [Vymazalová et al. \(2014a\)](#), IMA No 2013-115

Note: The structural identity between natural and synthetic Pd₁₄Ag₂Te₉ was confirmed by electron backscatter diffraction (EBSD).

Experimental: Phase relations in the system Pd-Ag-Te were determined at 350°C and 450°C ([Vymazalová et al., 2015](#)). At 350°C the system contains five ternary compounds: sopcheite (Pd₃Ag₄Te₄), lukkulaisvaaraite (Pd₁₄Ag₂Te₉), telargpalite (Pd_{2-x}Ag_{1+x}Te 0.09 < x < 0.22), and phases Pd_{7.5-x}Ag_{0.5+x}Te₃ (0.02 < x < 0.83) and Pd_{2+x}Ag_{2-x}Te (0.18 < x < 0.24). Lukkulaisvaaraite coexists with kotulskite and sopcheite, hessite and sopcheite, telargpalite and hessite; it forms stable associations with the phase Pd₃Te₂ and kotulskite, and with Pd₃Te₂ and telluropalladinite. It also coexists with a phase Pd_{7.5-x}Ag_{0.5+x}Te₃ and telargpalite, with the phase Pd_{7.5-x}Ag_{0.5+x}Te₃ and telluropalladinite. At 450°C, sopcheite is no longer stable and the assemblage lukkulaisvaaraite + kotulskite + hessite become stable.

10.5.12 MALYSHEVITE PDCUBIS₃

Crystallography: Orthorhombic, *Pnam*

Unit cell: $a = 7.541$, $b = 6.4823$, $c = 11.522$ Å, $V = 563.204$ Å³, $Z = 4$

X-ray powder diffraction pattern, strongest lines [d in Å(I)(hkl)]: 3.24(4)(020), 2.88(8)(004), 2.52(6)(300), 1.900(10)(304), 1.715(2)(206), 1.672(2)(225), ICDD PDF2 card—00-060-0390.

Structure: not determined, chemically Pd-analogue of lisiguangite

Appearance: Malyshevite forms rims (1–20 µm) around clauthalite, replacing padmaite.

Optical properties: In reflected light, white, bireflectance moderate, a bright yellow to pale yellow pleochroism; anisotropy weak to distinct (light yellow tints).

Reflectance, [\lambda nm, R ₁ R ₂ %]	470	34.1	28.7
	546	36.3	33.0
	589	37.0	34.4
	650	37.4	34.6

Physical Properties: Bluish gray, with metallic luster and gray streak.

Hardness: VHN not measured, Mohs 3

Cleavage: not observed

Density: 6.025 g/cm³ (calc.)

Chemical Composition (EMPA data, wt.%):

Pd 20.6, Pt 1.0, Pb 0.8, Bi 42.6, Cu 13.1, Se 2.2, S 19.0 \sum 99.3 (Pd_{0.94}Pt_{0.02}Pb_{0.02}) \sum 0.98Bi_{0.99}Cu_{1.00}(S_{2.88}Se_{0.14}) \sum 3.02 (*n* = 7)

Pd 22.39, Cu 13.38, Bi 43.99, S 20.24 \sum 100.00 PdBiCuS₃—ideal

Type locality and occurrence: The Srednyaya Padma U-V deposit in Southern Karelia, Russia. The mineral also observed in Cu-Ni-PGE ores in the footwall of the Sudbury Igneous Complex, Canada (Pentek et al., 2013), and in Noril'sk ores (Spiridonov et al., 2015) and is found in intergrowths with its Pt-analogue lisingsuaite from its type locality (Yu et al., 2009).

Name: In honor of I.I.Malyshev (1904–1973) and V.I. Malyshev (1927–2002), father (who first discovered the Malyshevskoe—Samotkanskoe Ti deposit) and son, formerly of the All-Russian Scientific-Research Institute of Mineral Resources (VIMS).

Reference: Chernikov et al. (2006), IMA No 2006-012

Note: Further investigations of the crystal structure are needed.

Experimental: The quaternary system Cu-Pd-Bi-S has not been experimentally studied.

10.5.13 MIESSIITE PD₁₁TE₂SE₂

Crystallography: cubic, *Fd* $\bar{3}$ *m*

Unit cell: *a* 12.448 Å, *V* 1929.0 Å³, *Z* = 8

X-ray powder diffraction pattern, strongest lines [*d* in Å(I)(*hkl*)]: 2.395(80)(511,333), 2.197(100)(440), 1.875(25)(622), 1.555(25)(800), 1.305(25)(931), 1.271(30)(844), ICDD PDF2 card—00-059-0323.

Structure: Isostructural with isomertierite (Pd₁₁As₂Sb₂) and törnroosite (Pd₁₁As₂Te₂).

Appearance: Discovered with placer gold and PGM nuggets, as one grain (483 × 522 µm). Shows a subidiomorphic cubic morphology.

Optical properties: In reflected light, light gray, isotropic.

Reflectance, [\lambda nm, R%]	470	48.88
	546	51.63
	589	53.91
	650	56.82

Physical Properties: Opaque, black with a metallic luster, malleable.

Hardness: VHN₁₀₀ 362 (348–370) g/mm², Mohs 2–2½

Cleavage: not observed

Density: 10.94 g/cm³ (calc.)

Chemical Composition (EMPA data, wt.%):

Pd 75.17, Te 17.06, Se 9.61 \sum 101.84 Pd_{11.02}Te_{2.09}Se_{1.90} ($n = 16$)

Pd 73.91, Te 16.12, Se 9.97 \sum 100.00 Pd₁₁Te₂Se₂—ideal

Type locality and occurrence: The Miessijoki River in the Lemmenjoki area, Inari commune, Finnish Lapland, Finland (25°21' N, 68°25' E).

Name: For the Miessi river, Finnish Lapland (in the Saami language “Miessijohka,” where *johka* means river, and *miessi* a reindeer calf).

Reference: Kojonen et al. (2007), IMA No 2006-013

Experimental: The synthetic analogue has not been studied; nor has the Pd-Te-Se system.

10.5.14 MILOTAITE PDSBSE

Crystallography: cubic, $P2_13$

Unit cell: $a = 6.3181 \text{ \AA}$, $V = 252.20 \text{ \AA}^3$, $Z = 4$

X-ray powder diffraction pattern, strongest lines [d in Å(I)(hkl)]: 2.825(100)(201), 1.905(98) (311), 2.579(81)(211), 3.159(53)(200), 2.233(32)(220), 1.752(27)(320), 1.688(25)(312), 1.378(18) (412), ICDD PDF2 card—01-073-3935, synth.

Structure: The crystal structure was determined on a single crystal of synthetic PdSbSe. The structure of PdSbSe is a homeotype of the structure of pyrite (FeS₂) and an isotype of the cubic ordered structure of gersdorffite (NiAsS).

Appearance: Occurs as subhedral grains (less than 25 µm in diameter), embedded in eucairite and tiemannite, randomly intergrown with a graphic intergrowth of bornite and selenian digenite.

Optical properties: In reflected light, white, isotropic.

Reflectance, [\lambda nm, R%]	470	nat.	48.6	synth.	48.0
	546		47.5		47.1
	589		47.6		47.0
	650		49.0		48.2

Physical Properties: Silvery gray, metallic luster, opaque, brittle, uneven fracture (synth.).

Hardness: VHN₁₀₀ 465 (420–514) g/mm² (synth.), Mohs 4½

Cleavage: not observed

Density: 8.09 g/cm³ (calc.), 7.98–8.23 g/cm³ (meas. on synth.)

Chemical Composition (EMPA data, wt.%):

Pd 34.17, Cu 0.78, Ag 0.35, Sb 38.03, Se 26.38 \sum 99.71 (Pd_{0.98}Cu_{0.04}) \sum 1.02(Ag_{0.01}Sb_{0.95}) \sum 0.96 Se_{1.02} ($n = 5$)

Pd 34.46, Sb 38.86, Se 26.60 \sum 99.91 Pd_{0.99}Sb_{0.97}Se_{1.04} (synth., $n = 17$)

Pd 34.65, Sb 39.64, Se 25.71 \sum 100.00 Pd₁Sb₁Se₁—ideal

Type locality and occurrence: Předbořice, a low-temperature selenide-bearing uranium mineralization in the Czech Republic.

Name: For Milota Makovicky (b. 1941), University of Copenhagen, in recognition of her investigations of sulfide and sulfoarsenide systems with PGE.

Reference: Paar et al. (2005), IMA No 2003-056

Note: X-ray powder-diffraction pattern derived from the crystal structure refinement. Identity between natural and synthetic PdSbSe confirmed by optical properties, reflectance data and chemical analyses.

Experimental: The ternary system Pd-Sb-Se has not been studied yet. Our preliminary experimental results of on-going research have shown that milotaita forms stable association with pallad-seite ($Pd_{17}Se_{15}$) and antimonselite (Sb_2Se_3), and coexists with stibiopalladinite (Pd_5Sb_2) at 400°C.

10.5.15 NALDRETTITE Pd_2Sb

Crystallography: orthorhombic, $Cmc2_1$

Unit cell: $a = 3.3906$, $b = 17.5551$, $c = 6.957 \text{ \AA}$, $V = 414.097 \text{ \AA}^3$, $Z = 8$

X-ray powder diffraction pattern, strongest lines [d in $\text{\AA}(I(hkl))$]: 2.2454(100)(132), 2.0567(52)(043), 2.0009(40)(152), 1.2842(42)(115), 1.2122(50)(204), 0.8584(56)(1174), ICDD PDF2 card—00-058-0460.

Structure: isostructural with Pd_2As

Appearance: Occurs as anhedral grains (varying in size from 10 to 239 μm), commonly attached or molded to sulfide minerals, also associated with clinochlor, rarely with magnetite.

Optical properties: In reflected light, bright creamy white, weak bireflectance, no pleochroism, distinct anisotropy (rotation tints deep bright blue, lemon-buff, and mauve pale pink); higher reflectance and less yellow against pentladite.

Reflectance, [λ nm, R ₁ R ₂ %]	470	air 49.0 50.9	im 35.9 37.6
	546	53.2 55.1	40.3 42.1
	589	55.4 57.5	42.5 44.3
	650	58.5 60.1	45.4 47.2

Physical Properties: Opaque, metallic, irregular fracture.

Hardness: VHN₅₀ 393 (358–418) g/mm², Mohs 4–5

Cleavage: not observed

Density: 10.694 g/cm³ (calc.)

Chemical Composition (EMPA data, wt.%):

Pd 63.49, Fe 0.11, Sb 35.75, As 0.31, S 0.02 $\sum 99.68$ ($Pd_{1.995}Fe_{0.007}$) $\sum 2.002$
($Sb_{0.982}As_{0.014}S_{0.002}$) $\sum 0.998$ ($n = 69$)

Pd 63.61, Sb 36.39 $\sum 100.00$ Pd_2Sb —ideal

Type locality and occurrence: The Mesamax Northwest deposit, Ungava region, Québec, Canada. It was also observed in the Tootoo and Mequillon magmatic sulfide deposits, New Quebec Orogen (Liu et al., 2013) and in concentrates of chromitite from the Korydallos area in the Pindos ophiolite complex, NW Greece (Kapsiotis et al., 2010). Observed as an unnamed phase in Cu-Ni sulfide deposits in clinopyroxenite intruding Permian sandy shales and volcanics, NE China and in a serpentinite intrusion in Permian metamorphic rocks, SW China (Cabri, 1981b, UN1974-8), in PGE mineralization in the Alaskan-type intrusive complexes near Fifield, New South Wales, Australia (Johan et al., 1989), in the vein-type Cu-Ni sulfide ores of the Ioko-Dovyren massif, northern Baikal region, Russia (Rudashevsky et al., 2003), and in Noril'sk ores (unpubl. data).

Name: For Anthony J. Naldrett (b. 1933), professor at the University of Toronto, in recognition of his significant contributions to understanding the genesis of PGE deposits.

Reference: Cabri et al. (2005), IMA No. 2004-007

Experimental: The mineral has a synthetic analogue synthesized by Bälz and Schubert (1969), ICDD PDF2 01-074-6150 card, El-Boragy and Schubert (1971b) and Kim and Chao (1996). It melts incongruently at 580°C (Kim and Chao, 1996); below this temperature it coexists with Pd_5Sb_2 or PdSb .

10.5.16 NIELSENITE PdCu_3

Crystallography: Tetragonal, $P4mm$

Unit cell: $a = 3.7125$, $c = 25.62 \text{ \AA}$, $V = 353.2 \text{ \AA}^3$, $Z = 4$

X-ray powder diffraction pattern, strongest lines [d in $\text{\AA}(I(hkl))$]: 2.137(100)(117), 1.8596(70) (200), 1.8337(40)(0014), 1.3126(60)(220), 1.1188(55)(317), 1.0663(30)(2214), ICDD PDF2

Structure: considered to be isostructural with synthetic tetragonal PdCu_3 , space group $P4mm$, but may belong to the $P4/mmm$ group

Appearance: Occurs as discrete grains or in sulfide-bearing, droplet-shaped to irregular grains 5–50 μm in size.

Optical properties: In reflected light, bright creamy white, anisotropy not observed (due to grain orientation, parallel to c)

Reflectance, [λ nm, R' %]	470	air 57.6	im 47.5
	546	60.85	50.8
	589	62.8	53.0
	650	66.7	57.5

Physical Properties: Steel-gray with a metallic luster, black streak, sectile tenacity

Hardness: not measured

Cleavage: not observed

Density: 9.53 g/cm³ (calc.)

Chemical Composition (EMPA data, wt.%):

Pd 29.86, Pt 3.08, Au 3.70, Cu 61.96, Fe 0.59, Pb 0.17 $\sum 99.36$ ($\text{Pd}_{0.862}\text{Au}_{0.058}\text{Pt}_{0.049}\text{Fe}_{0.028}$
 $\text{Pb}_{0.003})\sum 1.00(\text{Cu}_{2.996}\text{Fe}_{0.004})\sum 3.00(n=11)$
 Pd 35.82, Cu 64.18 $\sum 100.00$ PdCu_3 —ideal

Type locality and occurrence: The Skaergaard intrusion, Kangerdlugssuaq area, Est Greenland (68°09'55" N, 31°41'02" W). Also, found in concentrates of chromitite from the Korydallos area in the Pindos ophiolite complex, NW Greece (Kapsiotis et al., 2010), in magnetite-bearing gabbroic rocks of the Freetown Layered Complex, Sierra Leone (Bowles et al., 2013) and in Au-Cu-Pd-type mineralization in dolerites from Alexandra Land Island of the Franz Josef Archipelago (Sklyarov et al., 2016).

Name: After Troels F.D. Nielsen (b. 1950), a geologist with the Geological Survey of Denmark and Greenland, in recognition of his field work in the Skaergaard intrusion and his mineralogical and metallurgical studies.

Reference: McDonald et al. (2008), IMA No.2004-046

Experimental: According to the study of Karup-Møller et al. (2008) the formation of the phase can be assumed to be a product of low-temperature re-equilibration, shown as a 1D-LPS (one-dimensional long-period superlattice LPS) phase in the Cu-Pd phase diagram formed below 500°C (Subramanian and Laughlin, 1991).

10.5.17 NORILSKITE $(\text{PD},\text{AG})_7\text{PB}_4$

Crystallography: trigonal, $P3_121$

Unit cell: $a = 8.9656$, $c = 17.2801$ Å, $V = 1202.92$ Å³, $Z = 6$

X-ray powder diffraction pattern, strongest lines [d in Å(I)(hkl)]: 3.2201(29)(023,203), 2.3130(91)(026,206), 2.2414(100)(220), 1.6098(28)(046,406), 1.3076(38)(246,462), 1.2942(18)(600), 1.2115(37)(2212,1213), 0.9626(44)(0612,6012).

Structure: Crystallizes in the $\text{Ni}_{13}\text{Ga}_3\text{Ge}_6$ structure type, related to nickeline. The crystal structure was solved and refined from the powder X-ray-diffraction data of synthetic $(\text{Pd},\text{Ag})_7\text{Pb}_4$.

Appearance: Forms anhedral grains in aggregates (up to about 400 µm) with polarite, zvyagintsevite, Pd-rich tetra-auricupride, Pd-Pt bearing auricupride, Ag-Au alloys, (Pb,As,Sb) bearing ato-kite, mayakite, Bi-Pb rich kotulskite and sperrylite in pentlandite, cubanite, and talnakhite.

Optical properties: In reflected light, orange-brownish pink, moderate to strong bireflectance, orange-pink to greyish-pink pleochroism, strong anisotropy (rotation tints from dull yellow to dull blue in partially crossed polars); no internal reflections.

Reflectance, [λ nm, R_o $R_{e'}$ %]	470	51.1	48.8
	546	56.8	52.2
	589	59.9	53.5
	650	64.7	55.5

Physical Properties: Gray with metallic luster and gray streak, brittle.

Hardness: VHN₂₀ 310 (296–342) g/mm², Mohs 4

Cleavage: not observed

Density: 12.99 g/cm³ (calc.)

Chemical Composition (EMPA data, wt.%):

Pd 44.33, Ag 2.68, Bi 0.33, Pb 52.34 \sum 99.68 ($\text{Pd}_{6.56}\text{Ag}_{0.39}\sum 6.97(\text{Pb}_{3.97}\text{Bi}_{0.03})\sum 4.00$ ($n = 16$)

Pd 42.95, Ag 3.87, Pb 53.51 \sum 100.33 ($\text{Pd}_{6.25}\text{Ag}_{0.56}\sum 6.81\text{Pb}_{4.00}$ (synth., $n = 8$)

Pd 43.93, Ag 3.43, Pb 52.64 \sum 100.00 ($\text{Pd}_{6.5}\text{Ag}_{0.5}\sum 7\text{Pb}_4$)—ideal based on crystal structure

Type locality and occurrence: The Mayak mine of the Talnakh deposit, Russia (69°30'20" N, 88°27'17" E). Also observed from the Komsomolsky mine of the Talnakh deposit and from the Zapolyarny (Trans-Polar) mine of the Norilsk I deposit (Sluzhenikin and Mokhov, 2015).

Name: For the Norilsk district, Russia. Almost half of all known named platinum-group minerals have been reported to occur in the Norilsk ores.

Reference: Vymazalová et al. (2017), IMA No 2015-008

Note: The structural identity between the natural and synthetic $(\text{Pd},\text{Ag})_7\text{Pb}_4$ was confirmed by electron back-scattering diffraction (EBSD).

Experimental: The phase was synthesized at 300°C. The system Pd-Ag-Pb was experimentally studied by [Sarah et al. \(1981\)](#) at 400°C. Based on the proposed phase diagram, norilskite forms a stable assemblage with zvyagintsevite (Pd_3Pb) and Pd-Ag alloy, and coexists with Pd-Pb phases Pd_5Pb_3 , $\text{Pd}_{13}\text{Pb}_9$, and PdPb .

10.5.18 PALLADOSILICIDE Pd_2Si

Crystallography: hexagonal, $P\bar{6}2m$

Unit cell: $a = 6.496$, $c = 3.433 \text{ \AA}$, $V = 125.5 \text{ \AA}^3$, $Z = 3$

X-ray powder diffraction pattern, strongest lines [d in \AA (I)(hkl)]: 2.3658(100)(111), 2.1263(37)(120), 2.1808(34)(021), 3.240(20)(110), 1.8752(19)030), 1.7265(12)(002), 1.3403(11)(122), 1.2089(10)(231) (synth.)

Structure: Fe_2P type

Appearance: Found in a heavy-mineral concentrate, grains ranging in size from 0.7 to 39.1 μm .

Optical properties: In reflected light bright creamy white, weak bireflectance, weak anisotropy (rotation tints in shades of light blue and olive green)

Reflectance, [λ nm, R ₁ R ₂ %]	470	air 49.6 52.7	im. 36.3 38.6
	546	51.2 53.8	37.6 39.5
	589	51.6 53.7	37.8 39.5
	650	51.7 53.3	37.9 39.3

Physical Properties: Has an anhedral to subhedral habit, metallic luster.

Hardness: not measured

Cleavage: not observed

Density: 9.562-9.753 g/cm³ (calc.)

Chemical Composition (EMPA data, wt.%):

Si 7.95, Pd 68.56, Ag 1.07, Ni 4.59, Te 0.32 Sb 0.36, As 3.95, Fe 0.64, Pt 1.72, Sn 1.79, Cu 2.18, Rh 2.39 \sum 95.53 ($\text{Pd}_{1.657}\text{Ni}_{0.201}\text{Cu}_{0.088}\text{Rh}_{0.06}\text{Fe}_{0.029}\text{Ag}_{0.026}\text{Pt}_{0.023}\text{Sn}_{0.039}$) \sum 2.123(Si_{0.728}As_{0.136}Sb_{0.008}Te_{0.006}) \sum 0.878 (n = 8)—Kapalagulu

Si 10.13, Pd 68.77, Ag 0.33, Ni 5.16, Sb 0.11, As 2.18, Fe 0.35, Pt 4.45, Sn 3.08, Cu 1.62, Rh 3.76 \sum 99.94 ($\text{Pd}_{1.557}\text{Ni}_{0.212}\text{Cu}_{0.061}\text{Rh}_{0.088}\text{Fe}_{0.015}\text{Ag}_{0.007}\text{Pt}_{0.055}\text{Sn}_{0.063}$) \sum 2.058(Si_{0.869}As_{0.07}Sb_{0.002}) \sum 0.941 (n = 12)—UG-2

Pd 88.34 Si 11.66 \sum 100.00 Pd_2Si —ideal

Type locality and occurrence: PGE-chromite horizon of the Kapalagulu Intrusion near eastern shore of Lake Tanganyika, western Tanzania (30°03'51" E, 5°53'16" S and 30°05'37" E, 5°54'26" S) and the UG-2 chromitite, Bushveld Complex.

Name: For the chemical composition: Pd, Si.

Reference: [Cabri et al. \(2015\)](#), IMA No. 2014-080

Note: The structural identity of natural and synthetic Pd_2Si ([Nylund, 1966](#)) was confirmed by electron back-scattering diffraction (EBSD).

Experimental: The synthetic analogue melts congruently at 1330°C. [Langer and Wachtel \(1981\)](#) also observed a metastable state in the system, depending on the rate of cooling.

10.5.19 PAŠAVAITE $\text{Pd}_3\text{Pb}_2\text{Te}_2$

Crystallography: orthorhombic, $Pmmn$

Unit cell: $a = 8.599$, $b = 5.9381$, $c = 6.3173 \text{ \AA}$, $V = 322.6 \text{ \AA}^3$, $Z = 2$.

X-ray powder diffraction pattern, strongest lines [d in $\text{\AA}(I)(hkl)$]: 6.3152(34)(001), 3.1572(33)(002), 3.0495(100)(211), 2.5456(63)(202), 2.4424(34)(220), 2.2786(42)(221), 2.1637(71)(022), 2.1496(30)(400), 1.8906(42)(203), 1.5248(31)(422), ICDD PDF2 card—01-077-9121, synth.

Structure: Solved and refined from the powder X-ray diffraction data of synthetic $\text{Pd}_3\text{Pb}_2\text{Te}_2$. Structurally related to shandite ($\text{Ni}_3\text{Pb}_2\text{S}_2$) and parkerite ($\text{Ni}_3\text{Bi}_2\text{S}_2$).

Appearance: Occurs as subhedral grains (less than $20 \mu\text{m}$ in diameter) embedded in polarite, randomly accompanied by Pd-Pb-Bi-Te phases, sperrylite or intergrown with Au-Ag phases.

Optical properties: In reflected light, pale pink with brownish tinge, strong bireflectance, pleochroic from brownish to light pink, anisotropy distinct to strong, exhibits no internal reflections.

Reflectance, [λ nm, R ₁ R ₂ %]	470	nat. 42.4	synth. 49.9
	546	44.6	51.8
	589	45.7	52.2
	650	46.9	52.8

Physical Properties: Opaque, gray with metallic luster and gray streak, brittle (synth.).

Hardness: VHN_{25} 233 (173–281), Mohs 2

Cleavage: {001} weak

Density: 10.18 g/cm^3 (calc.), 9.9 g/cm^3 (meas. on synth.)

Chemical Composition (EMPA data, wt.%):

$\text{Pd} 31.51$, $\text{Pb} 41.54$, $\text{Bi} 0.19$, $\text{Te} 25.75 \sum 98.99 \text{ Pd}_{2.96}(\text{Pb}_{2.01}\text{Bi}_{0.01})\text{Te}_{2.02}$ ($n = 4$)

$\text{Pd} 32.17$, $\text{Pb} 41.78$, $\text{Te} 25.93 \sum 99.88 \text{ Pd}_{2.99}\text{Pb}_{2.00}\text{Te}_{2.01}$ (synth., $n = 7$)

$\text{Pd} 32.28$, $\text{Pb} 41.91$, $\text{Te} 25.81 \sum 100.00 \text{ Pd}_3\text{Pb}_2\text{Te}_2$ —ideal

Type locality and occurrence: The Talnakh deposit, Norilsk-Talnakh Ni-Cu camp, Taimyr Autonomous District, Russia.

Name: For Jan Pašava (b. 1957) of the Czech Geological Survey, in recognition of his contributions to the mineralogy and geochemistry of PGE in anoxic environments and other related ore deposits.

Reference: [Vymazalová et al. \(2009\)](#), IMA No 2007-059

Note: The structural identity of natural and synthetic $\text{Pd}_3\text{Pb}_2\text{Te}_2$ was confirmed by electron back-scattering diffraction (EBSD).

Experimental: Phase relations in the system Pd-Pb-Te were determined at 400°C (Vymazalová and Drábek, 2011); the Pd-rich corner at 480°C was explored by [El-Boragy and Schubert \(1971b\)](#). At 400°C the system contains two ternary compounds: pašavaite and $\text{Pd}_{71}\text{Pb}_8\text{Te}_{21}$ (not known to occur in nature). Pašavaite forms a stable assemblage with kotulskite solid-solution (25–30 at.% Pb) and altaite (PbTe). Pašavaite melts at 500°C .

10.5.20 SKAERGAARDITE PDCu

Crystallography: cubic, $Pm\bar{3}m$

Unit cell: $a = 3.0014 \text{ \AA}$, $V = 27.0378 \text{ \AA}^3$, $Z = 1$

X-ray powder diffraction pattern, strongest lines [d in Å(I)(hkl)]: 2.122(100)(110), 1.5000(20)(200), 1.2254(20)(211), 0.9491(20)(310), 0.8666(10)(222), 0.8021(70)(321), ICDD PDF2 card—00-057-0606.

Structure: CsCl-type. Isostructural with wairauite (CoFe), synthetic CuZn (β -brass) and structurally related to hongshiite (PtCu).

Appearance: Occurs as droplets, equant grains with rounded outlines, subhedral to euhedral crystals and irregular grains, in size from 2 to 75 μm .

Optical properties: In reflected light, bright creamy white (against to bornite and chalcopyrite), bright white (against digenite and chalcocite), isotropic.

Reflectance, [λ nm, R ₁ R ₂ %]	470	air 58.65	im. 47.4
	546	62.6	51.1
	589	64.1	52.8
	650	65.25	53.95

Physical Properties: Steel gray with a bronze tint, metallic luster, sectile.

Hardness: VHN₂₅ 257 (244–267) g/mm², Mohs 4–5

Cleavage: not observed

Density: 10.64 g/cm³ (calc.)

Chemical Composition (EMPA data, wt.%):

Pd 58.94, Pt 1.12, Au 2.23, Cu 29.84, Fe 3.85, Zn 1.46, Sn 1.08, Te 0.28, Pb 0.39 \sum 99.19
 $(\text{Pd}_{0.967}\text{Au}_{0.020}\text{Pt}_{0.010})_{\sum 0.997}(\text{Cu}_{0.820}\text{Fe}_{0.120}\text{Zn}_{0.039}\text{Sn}_{0.016}\text{Te}_{0.004}\text{Pb}_{0.003})_{\sum 1.002} (n=311)$
 Cu 37.39 Pd 62.61 \sum 100.00 CuPd—ideal

Type locality and occurrence: The Skaergaard intrusion, Kangerdlugssuaq area, East Greenland. Also found in a heavy-mineral concentrate from the Marathon deposit, Coldwell Complex, Canada (McDonald et al., 2015). Observed in concentrates of chromitite from the Korydallos area in the Pindos ophiolite complex, NW Greece (Kapsiotis et al., 2010); in Au-Cu-Pd-type mineralization in dolerites from Alexandra Land Island of the Franz Josef Archipelago (Sklyarov et al., 2016); in PGE mineralization in the Kirakkajuppura PGE deposit, Penikat layered complex, Finland (Barkov et al., 2005), and from the J-M reef, Stillwater Complex (Godel and Barnes, 2008).

Name: For the Skaergaard intrusion in East Greenland.

Reference: Rudashevsky et al. (2004), IMA No. 2003-049

Experimental: The transformation from disordered (Cu,Pd) solid solution to ordered CuPd occurs over the range 35–50 at.% Pd at 596°C (Subramanian and Laughlin, 1991).

10.5.21 TÖRNROOSITE PD₁₁AS₂TE₂

Crystallography: cubic, $Fd\bar{3}m$

Unit cell: a 12.3530, V 1885.03 Å³, Z = 8

X-ray powder diffraction pattern, strongest lines [d in Å(I)(hkl)]: 2.182(100)(440), 2.376(90)(511,333), 1.544(15)(800), 1.862(13)(622), 1.2606(13)(844), 1.608(11)(731,553)

Structure: Isostructural with isomertierite (Pd₁₁As₂Sb₂) and miessiite (Pd₁₁Se₂Te₂).

Appearance: Observed as an anhedral grain (size 132 x 200 µm), discovered with placer gold and PGM nuggets.

Optical properties: In reflected light yellowish white, isotropic.

Reflectance, [\lambda nm, R%]	470	45.4
	546	51.0
	589	54.1
	650	57.45

Physical Properties: Black, opaque with metallic luster, silvery black streak, malleable.

Hardness: VHN₂₅ 519 (509–536) kg/mm², Mohs 5.

Cleavage: not reported

Density: 11.205 g/cm³ (calc.)

Chemical Composition (EMPA data, wt.%):

Pd 72.04, Pt 1.75, Sb 2.13, Sb 0.85, As 8.77, Te 13.15, Bi 0.79 \sum 99.48 (Pd_{10.85}Pt_{0.14}) \sum 10.99
(As_{1.88}Sb_{0.11}) \sum 1.99 (Te_{1.65}Sn_{0.29}Bi_{0.06}) \sum 2.00 ($n = 10$)
Pd 72.29, As 9.51, Te 16.20 \sum 100.00 Pd₁₁As₂Te₂—ideal

Type locality and occurrence: The Miessijoki River, Lemmenjoki area, Inari Commune, Finnish Lapland, Finland (25°42'33" N, 68°42'30" E). Also observed in a heavy-mineral concentrate from the Marathon Cu-PGE-Au deposit, Coldwell Complex, Ontario, Canada (McDonald et al., 2015) and in the sulfide-bearing pegmatoidal pyroxenites of the South Sopcha intrusion of the Monchegorsk Igneous Complex, Kola peninsula, Russia (Grokhovskaya et al., 2012), in PGE mineralization of the Fedorova-Pana ore node (Subbotin et al., 2012) and as an unnamed phase in PGE concentrate from alluvial sediments from the farm Maandagshoek in the eastern Bushveld (Oberthür et al., 2004).

Name: For Ragnar Törnroos (b. 1943), University of Helsinki, for his pioneering research on placer PGM in Finnish Lapland and his contributions to ore mineralogy.

Reference: Kojonen et al. (2011), IMA No 2010-043

Note: The crystal structure of törnroosite was refined on a single crystal sample from the South Sopcha intrusion, Russia by Karimova et al. (2016), the data are in an agreement with those proposed by Kojonen et al. (2011).

Experimental: The synthetic analogue is not known. The system Pd-As-Te was experimentally studied by El-Boragy and Schubert (1971b) at 480°C, but it requires some further re-examination, particularly in the Pd-rich corner, reflecting new observations in the binary systems Pd-Te and Pd-As. The phase assigned as Pd₆AsTe by El-Boragy and Schubert (1971b) could be in fact Pd₁₁As₂Te₂.

10.5.22 UNGAVAITE PD₄SB₃

Crystallography: tetragonal, P4₁2₁2, P4₁22, P4₃2₁2, P4₂2₁2 or P4₂22

Unit cell: $a = 7.7388$, $c = 24.145$ Å, $V = 1446.02$ Å³, $Z = 8$

X-ray powder diffraction pattern, strongest lines [d in Å(I)(hkl)]: 3.008(90)(008), 2.268(100)
(134), 2.147(30)(230), 1.9404(60)(400), 1.2043(30)(2218,452), 1.2002(30)(624), ICDD PDF2 card—00-058-0505.

Structure: not determined

Appearance: Occurs as rare anhedral grains with inclusions of Au-Ag alloy or with attached chalcopyrite and a chlorite-group mineral, from 36 to 116 μm in size.

Optical properties: In reflected light, bright creamy white, weak bireflectance, no pleochroism, weak anisotropy (rotation tints pale blue-gray to deep blue).

Reflectance, [λnm , R ₁ R ₂ %]	470	air 50.2 50.5	im. 37.6 38.0
	546	55.6 55.9	43.2 43.5
	589	57.9 58.3	45.9 46.3
	650	60.2 60.7	48.1 48.5

Physical Properties: Opaque, dark gray, metallic, malleable.

Hardness: not measured

Cleavage: not observed

Density: 7.264 g/cm³ (calc.)

Chemical Composition (EMPA data, wt.%):

Pd 54.53, Fe 0.13, Te 0.09, Sb 44.59, Bi 0.42 Hg 0.19 As 0.20 \sum 100.15
 $\text{Pd}_{4.062}(\text{Sb}_{2.893}\text{Fe}_{0.017}\text{Bi}_{0.017}\text{Hg}_{0.006}\text{Te}_{0.005})_{\sum 2.938}$ ($n = 16$)
 Pd 53.82 Sb 46.18 \sum 100.00 Pd₄Sb₃—ideal

Type locality and occurrence: The Mesamax Northwest Ni-Cu-Co-PGE deposit in the Cape Smith fold belt of the Ungava region, northern Quebec, Canada (61°34'25" N, 73°15'36" W). Also observed in the Tootoo and Mequillon magmatic sulfide deposits, New Quebec Orogen ([Liu et al., 2013](#)).

Name: After the locality in the Ungava region, Quebec, Canada.

Reference: [McDonald et al. \(2005\)](#), IMA No. 2004–020

Note: Some further experimental and crystal structure investigations are needed.

Experimental: The synthetic analogue is not known from the experimental studies related to Pd-Sb system ([El-Boragy and Schubert, 1971b](#)), nor from studies on ternary systems involving Pd and Sb including those made by [Kim and Chao \(1991, 1996\)](#), [Cabri et al. \(1975\)](#).

10.5.23 ZACCARINIITE RHNIAS

Crystallography: tetragonal, $P4/nmm$

Unit cell: $a = 3.5498$, $c = 6.1573 \text{ \AA}$, $V = 77.59 \text{ \AA}^3$, $Z = 2$

X-ray powder diffraction pattern, strongest lines [d in $\text{\AA}(I)(hkl)$]: 2.5092(40)(110), 2.3252(100) (111,102), 1.9453(51)(112), 1.7758(80)(103,200), 1.2555(40)(213,220), 1.1044(22)(302,311), 1.0547(23)(312), 0.9730(42)(215). (synth.)

Structure: Cu₂Sb type. The crystal structure was refined from the powder XRD data of synthetic RhNiAs using the initial structural model of [Roy-Montreuil et al. \(1984\)](#), ICSD card No187596.

Appearance: Forms anhedral grains (1–20 μm in size), intergrown with garutite, in association with hexaferrum, Ru-Os-Ir-Fe alloys, and Ru-Os-Ir-Fe oxygenated compounds in chromite.

Optical properties: In reflected light, white with brownish to pinkish tints, has moderate to strong bireflectance, a strong white to pinkish brownish white pleochroism, strong anisotropy (with rotation tints from orange to blue-green); exhibits no internal reflections.

<i>Reflectance, [λnm, R₁ R₂ %]</i>	470	nat. 49.4 52.6	synth. 49.1 53.3
	546	52.4 53.2	53.1 54.1
	589	54.2 53.2	55.2 53.9
	650	56.6 53.3	57.9 53.9

Physical Properties: Opaque, metallic luster, gray streak, brittle.

Hardness: VHN₅ 218 (166–286) g/mm², Mohs 3½–4

Cleavage: not observed

Density: 10.19 g/cm³ (calc.), 10.09 g/cm³ (meas. on synth.)

Chemical Composition (EMPA data, wt.%):

Rh 41.77, Os 0.51, Ir 0.64, Ru 0.46, Pd 0.34, Ni 23.75, Fe 0.53, As 27.84, S 0.10, \sum 96.09 wt.%, $(\text{Rh}_{1.01}\text{Os}_{0.01}\text{Ir}_{0.01}\text{Ru}_{0.01}\text{Pd}_{0.01})_{\sum 1.05}(\text{Ni}_{1.00}\text{Fe}_{0.02})_{\sum 1.02}(\text{As}_{0.92}\text{S}_{0.01})_{\sum 0.93(n=3)}$
 Rh 44.57, Ni 24.50, As 31.82 \sum 100.88 Rh_{1.02}Ni_{0.98}As_{1.00} (synth., n = 28)
 Rh 43.51, Ni 24.82, As 31.67 \sum 100.00 RhNiAs—ideal

Type locality and occurrence: The Loma Peguera ophiolitic chromitite, Dominican Republic.

It has been observed from several localities worldwide, e.g., the Guli chromitite, Ray-Iz ophiolite complex, Nizhny Tagil, the ophiolitic belt in the Koryak-Kamchatska fold region in Russia, the Thetford Mines in Canada, the Vourinos complex in Greece, and the Bushveld complex in South Africa.

Name: For Federica Zaccarini (b. 1962) of the University of Leoben, in recognition of her contributions to PGE mineralogy and related deposits.

Reference: [Vymazalová et al. \(2012b\)](#), IMA No. 2011-086

Note: The structural identity between the natural and synthetic RhNiAs was confirmed by Raman spectroscopy.

Experimental: The phase was synthesized at 800°C; the system Rh-As-Ni has not been experimentally investigated.

ACKNOWLEDGEMENTS

We are very grateful to Louis J. Cabri and Emil Makovicky for their detailed and helpful comments on the manuscript. We are grateful to Sisir K. Mondal and William L. Griffin for the editorial handling and for reading the final manuscript and correcting the English.

REFERENCES

- Airyants, E.V., Zhmodik, S.M., Ivanov, P.O., Belyanin, D.K., Agafonov, L.V., 2014. Mineral inclusions in Fe-Pt solid solution from the alluvial ore occurrences of the Anabar basin (northeastern Siberian Platform). Russian Geol. Geophys. 55 (8), 945–958.
- Baghdadi, A., Finley, A., Russo, P., Arnott, R.J., Wold, A., 1974. Crystal growth and characterization of PtP₂. J. Less Common Metals 34 (1), 31–38.
- Bälz, U., Schubert, K., 1969. Crystal structure of Pd₂As and Pd₂Sb (r). J. Less-Common Met. 19, 300–304, in German.

- Baranov, A.I., Isaeva, A.A., Kloo, L., Popovkin, B.A., 2003. New metal-rich sulfides Ni_6SnS_2 and $\text{Ni}_9\text{Sn}_2\text{S}_2$ with a 2D metal framework: synthesis, crystal structure, and bonding. *Inorg. Chem.* 42, 6667–6672.
- Baranov, A.I., Isaeva, A.A., Kloo, L., Kulbachinskii, V.A., Lunin, R.A., Nikiforov, V.N., et al., 2004. 2D metal slabs in new nickel-tin chalcogenides $\text{Ni}_{7-8}\text{SnQ}_2$ ($\text{Q} = \text{Se}, \text{Te}$): average crystal and electronic structures, chemical bonding and physical properties. *J. Solid State Chem.* 177, 3616–3625.
- Barkov, A.Y., Fleet, M.E., Martin, R.F., Halkoaho, T.A.A., 2005. New data on “bonanza”-type PGE mineralization in the Kirakkajuppura PGE deposit, Penikat layered complex, Finland. *Can. Mineral.* 43 (5), 1663–1686.
- Beck, J., Hilbert, T., 2000. An “old” rhodiumsulfide with surprising structure – synthesis, crystal structure, and electronic properties of Rh_3S_4 . *Z. Anorg. Allg. Chem.* 626, 72–79.
- Bennett, S.L., Heyding, R.D., 1966. Arsenides of the transitions metals. VIII. Some binary and ternary group VIII Diarsenides and their magnetic and electrical properties. *Can. J. Chem.* 44, 3017–3036.
- Berlincourt, L.E., Hummel, H.H., Skinner, B.J., 1981. Phases and phase relations of the platinum-group elements. In: Cabri, L.J. (Ed.), *Platinum Group Elements: Mineralogy, Geology, Recovery*, CIM Special Vol, 23. pp. 19–45.
- Bichsel, R., Levy, F., Berger, H., 1984. Growth and physical properties of RuS_2 single crystals. *J. Physics C: Solid State Phys.* 17 (1), L19–L21.
- Bindi, L., 2010. Atheneite, $\text{Pd}_2\text{As}_{0.75}\text{Hg}_{0.25}$ from Itabira mines, Mina Gerais, Brazil: crystal structure and revision of the chemical formula. *Can. Mineral.* 48 (5), 1149–1155.
- Botelho, N.F., Moura, M.A., Peterson, R.C., Stanley, C.J., Silva, D.V.G., 2006. Kalungaite, PdAsSe , a new platinum-group mineral from the Buraco do Ouro gold mine, Cavalcante, Goiás State, Brazil. *Mineral. Mag.* 70 (1), 123–130.
- Bowles, J.F.W., Prichard, H.M., Suarez, S., Fisher, P., 2013. The first report of platinum-group minerals in magnetite-bearing gabbro, Freetown layered complex, Sierra Leone: occurrences and genesis. *Can. Mineral.* 51 (3), 455–473.
- Brenner, S.S., 1956. The growth of whiskers by the reduction of metal salts. *Acta Metallurgica* 4 (1), 62–74.
- Bridgman, P.W., 1925. Certain physical properties of single crystals of tungsten, antimony, bismuth, tellurium, cadmium, zinc, and tin. *Proc. Am. Acad. Arts Sci.* 60 (6), 305–383.
- Bryukvin, V.A., Fishman, B.A., Reznichenko, V.A., Kuoev, V.A., Vasil'eva, N.A., 1990. Investigation of the Fe-Rh-S phase diagram in the Fe-Rh- Rh_2S_3 - $\text{FeS}_{1.09}$ compositional range. *Izvestiya Akademii Nauk SSSR. Metal'y.* 2, 23–28, in Russian.
- Bugaris, D.E., Malliakas, C.D., Shoemaker, D.P., Do, D.T., Chung, D.Y., Mahanti, S.D., et al., 2014. Crystal Growth and Characterization of the Narrow-Band-Gap Semiconductors OsPn_2 ($\text{Pn} = \text{P}, \text{As}, \text{Sb}$). *Inorg. Chem.* 53 (18), 9959–9968.
- Cabral, A.R., Skála, R., Vymazalová, A., Kallistová, A., Lehmann, B., Jedwab, J., et al., 2014. Kitagohaité, Pt_7Cu , a new mineral from the Lubero region, North Kivu, DR Congo. *Mineral. Mag.* 78 (3), 739–745.
- Cabri, L.J., 1973. New data on phase relations in Cu-Fe-S system. *Econ. Geol.* 68 (4), 443–454.
- Cabri, L.J., 1981a. The Platinum-group minerals. In: Cabri, L.J. (Ed.), *Platinum Group Elements: Mineralogy, Geology, Recovery*, CIM Special Vol, 23. pp. 83–150.
- Cabri, L.J., 1981b. Unnamed Platinum-group minerals. In: Cabri, L.J. (Ed.), *Platinum Group Elements: Mineralogy, Geology, Recovery*, CIM Special Vol, 23. pp. 175–186.
- Cabri, L.J., 2002. The Platinum-group minerals. In: Cabri, L.J. (Ed.), *The Geology, Geochemistry, Mineralogy and Mineral Beneficiation of Platinum-Group Elements*, CIM Special Vol, 54. pp. 177–210.
- Cabri, L.J., Laflamme, J.H.G., Stewart, J.M., Rowland, J.F., Chen, T.T., 1975. New data on some palladium arsenides and antimonides. *Can. Mineral.* 13, 321–335.
- Cabri, L.J., Chen, T.T., Stewart, J.M., Gilles, J.H., Laflamme, J.H.G., 1976. Two new palladium-arsenic-bismuth minerals from the Stillwater complex, Montana. *Can. Mineral.* 14, 410–413.

- Cabri, L.J., Laflamme, J.H.G., Stewart, J.M., Turner, K., Skinner, B.J., 1978. On cooperite, braggite, and vysotskite. *Am. Mineral.* 63, 832–839.
- Cabri, L.J., McDonald, A.M., Stanley, C.J., Rudashevsky, N.S., Poirier, G., Durham, B.R., et al., 2005. Naldrettite, Pd_2Sb , a new intermetallic mineral from the Mesamax Northwest deposit, Ungava region, Quebec, Canada. *Mineral. Mag.* 69 (1), 89–97.
- Cabri, L.J., McDonald, A.M., Stanley, C.J., Rudashevsky, N.S., Poirier, G., Wilhelmij, H.R., et al., 2015. Palladosilicide, Pd_2Si , a new mineral from the Kapalagulu Intrusion, Western Tanzania and the Bushveld Complex, South Africa. *Mineral. Mag.* 79 (2), 295–307.
- Campbell, I.E., Powell, C.F., Nowicki, D.H., Gonser, B.W., 1949. The Vapor-Phase Deposition of Refractory Materials I. General Conditions and Apparatus. *J. Electrochem. Soc.* 96 (5), 318–333.
- Canfield, P.C., Fisk, Z., 1992. Growth of single crystals from metallic fluxes. *Philosophical Magazine B* 65 (6), 1117–1123.
- Chareev, D.A., 2015. The low temperature electrochemical growth of iron, nickel and other metallic single crystals from halide eutectic fluxes in a temperature gradient. *J. Crystal Growth* 429, 63–67.
- Chareev, D.A., Volkova, O.S., Geringer, N.V., Koshelev, A.V., Nekrasov, A.N., Osadchii, V.O., et al., 2016. Synthesis of chalcogenide and pnictide crystals in salt melts using a steady-state temperature gradient. *Crystallog. Rep.* 61 (4), 682–691.
- Chernikov, A.A., Chistyakova, N.I., Uvarkina, O.M., Dubinchuk, V.T., Rassulov, V.A., Polekhovsky, Y.S., 2006. Malyshevite - a new mineral from Srednyaya Padma deposit in Southern Karelia. *New Data Mineral.* 41, 14–17, in Russian.
- Chernyaev, I.I., Zheligovskaya, N.N., Borisenkova, M.K., Subbotina, N.A., 1968. The Ag_2Te-Pd System. *Russ. J. Inorg. Chem.* 13, 848–850, in Russian.
- Chirvinskii, P.N., 1995. Artificial Formation of Minerals in the XIX Century. In: Zharikov, V.A. (Ed.), *Classics of Science*. Nauka, Moscow, p. 510. , in Russian.
- Clark, A.M., Criddle, A.J., Fejer, E.E., 1974. Palladium arsenide-antimonids from Itabira, Minas Gerais, Brazil. *Mineral. Mag.* 39, 528–543.
- Colell, H., Alonso-Vante, N., Fiechter, S., Schieck, R., Diesner, K., Henrion, W., et al., 1994. Crystal growth and properties of novel ternary transition metal chalcogenide compounds $Ir_xRu_{1-x}S_2$ ($0.005 < x < 0.5$). *Mater. Res. Bull.* 29 (10), 1065–1072.
- Czochralski, J., 1918. A new method for the measurement of the crystallization rate of metals. *Z. Physik. Chem.* 92, 219–221, in German.
- Dobersek, M., Kosovinc, I., 1989. The ternary system palladium-copper-zinc. *Z. Metallkd.* 80, 669–671, in German.
- Drábek, M., Rieder, M., 2008. The system Os-Mo-S. *Can. Mineral.* 46 (5), 1297–1303.
- Drábek, M., Vymazalová, A., Cabral, A.R., 2012. The Pt–Hg–Se system at 400°C: phase relations of jacutin-gaite. *Can. Mineral.* 50 (2), 441–446.
- Drábek, M., Vymazalová, A., Laufek, F., 2014. The system Hg–Pd–Se at 400°C: phase relations involving tischendorfite. *Can. Mineral.* 52 (2), 763–768.
- El-Boragy, M., Ellner, M., Schubert, K., 1984. On Several Phases of the Mixture $NiPd_xAs_x$. *Z. Metallkd.* 75, 82–85, in German.
- El-Boragy, M., Schubert, K., 1971a. Crystal structures of some ternary phases in T-B-B' systems. *Z. Metallkd.* 62, 667–675, in German.
- El-Boragy, M., Schubert, K., 1971b. On some variants of the NiAs family in mixtures of palladium with B-elements. *Z. Metallkd.* 62, 314–323, in German.
- Evstigneeva, T.L., Nekrasov, I.Y., 1980. Conditions of phase synthesis and phase relations in the systems Pd_3Sn-Cu_3Sn and $Pd-Sn-Cu-HCl$. In: Zharikov, V.A., Fedkin, V.V. (Eds.), *Sketches of Physico-Chemical Petrology*, 10. Nauka, Moscow, pp. 20–35. , in Russian.

- Ezzaouia, H., Heindl, R., Parsons, R., Tributsch, H., 1983. Visible light photo-oxidation of water with single-crystal RuS₂ electrodes. *J. Electroanal. Chem. Interfacial Electrochem.* 145 (2), 279–292.
- Ezzaouia, H., Heindl, R., Loriers, J., 1984. Synthesis of ruthenium and osmium dichalcogenide single crystals. *J. Mater. Sci. Lett.* 3 (7), 625–626.
- Ezzaouia, H., Foise, J.W., Gorochov, O., 1985. Crystal growth in tellurium fluxes and characterization of RuS₂ single crystals. *Mater. Res. Bull.* 20 (11), 1353–1358.
- Fiechter, S., Kühne, H.M., 1987. Crystal Growth of RuX₂ (X = S, Se, Te) by chemical vapour transport and high temperature solution growth. *J. Crystal Growth* 83 (4), 517–522.
- Finley, A., Schleich, D., Ackerman, J., Soled, S., Wold, A., 1974. Crystal growth and characterization of Pt_{0.97}S₂. *Mater. Res. Bull.* 9 (12), 1655–1659.
- Fisk, Z., Remeika, J.P., 1989. Growth of single crystals from molten metal fluxes. *Handbook Phys. Chem. Rare Earths* 12, 53–70.
- Foecker, A.J., Jeitschko, W., 2001. The atomic order of the pnictogen and chalcogen atoms in equiatomic ternary compounds TPnCh (T5 Ni, Pd; Pn 5 P, As, Sb; Ch 5 S, Se, Te). *J. Solid State Chem.* 162, 69–78.
- Foise, J.W., Ezzaouia, H., Gorochov, O., 1985. Crystal growth of p-type RuS₂ using bismuth flux and its photoelectrochemical properties. *Mater. Res. Bull.* 20 (12), 1421–1425.
- Georg, C.A., Triggs, P., Levy, F., 1982. Chemical vapour transport of transition metal oxides (I) crystal growth of RuO₂, IrO₂ and Ru_{1-x}Ir_xO₂. *Mater. Res. Bull.* 17 (1), 105–110.
- Gerville, F., Makovicky, E., Makovicky, M., Rose-Hansen, J., 1994. The system Pd-Ni-As at 790° and 450°C. *Econ. Geol.* 89, 1630–1639.
- Godel, B., Barnes, S.-J., 2008. Image analysis and composition of platinum-group minerals in the J-M reef, Stillwater Complex. *Econ. Geol.* 103 (3), 637–651.
- Grokhovskaya, T.L., Bakaev, G.F., Sholokhnev, V.V., Lapin, M.I., Muravitskaya, G.N., Voitekhovich, V.S., 2003. The PGE Ore Mineralization in the Monchegorsk Igneous Layered Complex (Kola Peninsula, Russia). *Geol. Rudnykh Mestorozhdenii* 45 (4), 329–352.
- Grokhovskaya, T.L., Lapina, M.I., Mokhov, A.V., 2009. Assemblages and genesis of platinum-group minerals in low-sulfide ores of the Monchetundra deposit, Kola peninsula, Russia. *Geol. Ore Deposits* 51 (9), 467–485.
- Grokhovskaya, T.L., Karimova, O.V., Griboedova, I.G., Samoshnikova, L.A., Ivanchenko, V.N., 2012. Geology, mineralogy and genesis of PGE mineralization in the South Sopcha massif, Monchegorsk complex, Russia. *Geol. Ore Deposit* 54, 347–369.
- Helmy, H.M., Ballhaus, C., Berndt, J., Bockrath, C., Wohlgemuth-Ueberwasser, C., 2007. Formation of Pt, Pd and Ni tellurides: experiments in sulfide-telluride systems. *Cont. Mineral. Petrol.* 153, 577–591.
- Hoffman, E., MacLean, W.H., 1976. Phase relations of michenerite and merenskyite in the Pd-Bi-Te system. *Econ. Geol.* 71, 1461–1468.
- Horkans, J., Shafer, M.W., 1977. An investigation of the electrochemistry of a series of metal dioxides with rutile-type structure: MoO₂, WO₂, ReO₂, RuO₂, OsO₂, and IrO₂. *J. Electrochem. Soc.* 124 (8), 1202–1207.
- Huang, J.K., Huang, Y.S., Yang, T.R., 1994. The preparation and characterization of RuTe₂ single crystals. *J. Crystal Growth* 135 (1), 224–228.
- Hurle, D.T.J., Mullin, J.B., Pike, E.R., 1967. Thin alloy zone crystallisation. *J. Material. Sci.* 2 (1), 46–62.
- Johan, Z., Ohnenstetter, M., Slansky, E., Barron, L.M., Suppel, D., 1989. Platinum mineralization in the Alaskan-type intrusive complexes near Fifield, New-south Wales, Australia Part1. Platinum-group minerals in clinopyroxenites of the Kelvin Grove Prospect, Owendale intrusion. *Miner. Petrol.* 40 (4), 289–309.
- Kaner, R., Castro, C.A., Gruska, R.P., Wold, A., 1977. Preparation and characterization of the platinum metal phosphides RuP₂ and IrP₂. *Material. Res. Bull.* 12 (12), 1143–1147.

- Kapsiotis, A., Grammatikopoulos, T.A., Tsikouras, B., Hatzipanagiotou, K., 2010. Platinum-group mineral characterization in concentrates from high-grade PGE Al-rich chromitites of Korydallos area in the Pindos Ophiolite Complex (NW Greece). *Resour. Geol.* 60 (2), 178–191.
- Karimova O.V., Zolotarev A.A., Evstigneeva T.L., Johanson B., Mertieite-II, $Pd_8Sb_{2.5}As_{0.5}$, crystal structure refinement and formula revision. *Mineral. Mag.* (in press).
- Karimova, O.V., Grokhovskaya, T.L., Zolotarev, A.A., Gurzhiy, V.V., 2016. Crystal structure refinement of isomertieite, $Pd_{11}Sb_2As_2$, and törnroosite, $Pd_{11}As_2Te_2$. *Can. Mineral.* 54 (2), 511–517.
- Karup-Møller, S., Makovicky, E., 2007. The system Cu-Rh-S at 900 °C, 700 °C, 540 °C and 500 °C. *Can. Mineral.* 45 (6), 1535–1542.
- Karup-Møller, S., Makovicky, E., Barnes, S.-J., 2008. The metal-rich portions of the phase system Cu-Fe-Pd-S at 1000 °C, 900 °C and 725 °C: implications for mineralization in the Skaergaard intrusion. *Mineral. Mag.* 72 (4), 941–951.
- Kim, W.S., 2009. Synthesis of Pt-Pd antimonide minerals at 1000 °C and the extent of Pt-Pd substitutions. *Geosci.* J 13 (1), 25–30.
- Kim, W.S., Chao, G.Y., 1991. Phase relations in the system Pd-Sb-Te. *Can. Mineral.* 29, 401–409.
- Kim, W., Chao, G.Y., 1996. Phase relations in the system Pd-Pt-Sb. *Neues Jahrb. Mineral., Monatsh.* 351–364.
- Kojonen, K.K., McDonald, A.M., Stanley, C.J., Johanson, B., 2011. Törnroosite, $Pd_{11}As_2Te_2$, a new mineral species related to isomertieite from Miessijoki, Finnish Lapland, Finland. *Can. Mineral.* 49, 1643–1652.
- Kojonen, K.K., Tarkian, M., Roberts, A.C., Tornroos, R., Heidrich, S., 2007. Miessite, $Pd_{11}Te_2Se_2$, a new mineral species from Miessijoki, Finnish Lapland, Finland. *Can. Mineral.* 45 (5), 1221–1228.
- Kullerud, G., 1971. Experimental techniques in dry sulfide research. In: Ulmer, G.C. (Ed.), *Research Techniques for High Pressure and High Temperature*, Springer-Verlag, New York, pp. 288–315.
- Kyropoulos, S., 1926. Ein Verfahren zur Herstellung grosser Kristalle. *Z. Anorg. Allgem. Chemie* 154 (1), 308–313, in German.
- Langer, H., Wachtel, E., 1981. Aufbau und Magnetische Eigenschaften von Palladium Silicium-Legierungen im Konzentrationsintervall 30 bis 100 at. % Si. *Z. Metallkd.* 72, 769–775.
- Laufek, F., Vymazalová, A., Drábek, M., Dušek, M., Navrátil, J., Černošková, E., 2016. The crystal structure of temagamite, Pd_3HgTe_3 . *Eur. J. Mineral.* 28, 825–834.
- Laufek, F., Vymazalová, A., Drábek, M., Navrátil, J., Drahokoupil, J., 2014. Synthesis and crystal structure of tischendorfite $Pd_8Hg_3Se_9$. *Eur. J. Mineral.* 25, 157–162.
- Laufek, F., Vymazalová, A., Grokhovskaya, T.L., Plášil, J., Dušek, M., Orsoev, D.A., Kozlov V.V. The Crystal Structure of sopcite, $Ag_4Pd_3Te_4$, from the Lukkulaisvaara intrusion, northern Russian Karelia, Russia *Eur. J. Mineral.* in press.
- Lebrun, N., Cacciamani, G., Cordes, H., Effenberg, G., Ilyenko, S., Schmid-Fetzer, R., 2007. Cu-Pb-Zn (Copper-Lead-Zinc).. In: Effenberg, G., Ilyenko, S. (Eds.), *Ternary Alloy Systems, Noble Metal Systems. Landolt-Börnstein - Group IV Physical Chemistry Series, 11B*. Springer Berlin Heidelberg, pp. 408–419.
- Liao, P.C., Ho, C.H., Huang, Y.S., Tiong, K.K., 1997. Preparation and characterization of pyrite-like single crystal phase in the Ir-Te system. *J. Crystal Growth* 171 (3), 586–590.
- Liu, Y., Mungall, J.E., Ames, D.E., 2013. Hydrothermal redistribution and local enrichment of platinum group elements in the Tootoo and Mequillon magmatic sulfide deposits, South Raglan Trend, Cape Smith Belt, New Quebec Orogen. *Econ. Geol.* 111 (2), 467–485.
- Lyons, A., Schleich, D., Wold, A., 1976. Crystal growth and characterization of $PdTe_2$. *Material. Res. Bull.* 11 (9), 1155–1159.
- Makovicky, E., 2002. Ternary and quaternary phase systems with PGE. In: Cabri, L.J. (Ed.), *The Geology, Geochemistry, Mineralogy and Mineral Beneficiation of Platinum-Group Elements*, CIM Special Vol, 54. pp. 131–175.

- Makovicky, E., Karup-Møller, S. Exploratory studies of the Cu-Pd-Se system from 300 to 650 °C, *Eur. J. Mineral.* in press.
- Makovicky, E., Karup-Møller, S., 2016. The Pd–Ni–Fe–S phase system at 550 and 400°C. *Can. Mineral.* 54 (2), 377–400.
- Makovicky, E., Makovicky, M., Rose-Hansen, J., 2002. The system Fe-Rh-S at 900° and 500 °C. *Can. Mineral.* 40, 519–526.
- Massalski, T.B., 1990. Binary Alloy Phase Diagrams. 2nd ed. ASM International, Materials Park, Ohio.
- Matsumoto, N., Nagata, S., 2000. Single-crystal growth of sulphospinel CuIr₂S₄ from Bi solution. *J. Crystal Growth* 210 (4), 772–776.
- McDonald, A.M., Ames, D.E., Ross, K.C., Kjarsgaard, I.M., Good, D.J., 2016. Marathonite, IMA 2016-080. CNMNC Newsletter No. 34, December 2016, page 1320. *Mineral. Mag.* 80, 1315–1321.
- McDonald, A.M., Cabri, L.J., Stanley, C.J., Rudashevsky, N.S., Poirer, G., Ross, K.C., et al., 2005. Ungavaite, Pd₄Sb₃, a new intermetallic mineral from the Mesamax Northwest Deposit, Ungava Region, Quebec, Canada. *Can. Mineral.* 43 (5), 1735–1744.
- McDonald, A.M., Cabri, L.J., Rudashevsky, N.S., Stanley, C.J., Rudashevsky, V.N., Ross, K.C., 2008. Nielsenite, PdCu₃, a new platinum-group intermetallic mineral from the Skaergaard intrusion, Greenland. *Can. Mineral.* 46, 709–716.
- McDonald, A.M., Cabri, L.J., Stanley, C.J., Good, D.J., Redpath, J., Spratt, J., 2015. Coldwellite, Pd₃Ag₂S, a new mineral species from the Marathon deposit, Coldwell Complex, Ontario, Canada. *Can. Mineral.* 53, 845–857.
- McDonald, A.M., Zhe, W., Ames, D.E., Ross, K.C., Kjarsgaard, I.M., Good, D.J., 2017. Palladogermanide, IMA 2016-086. CNMNC Newsletter No. 35, February 2017, page 210. *Mineral. Mag.* 81, 209–213.
- Mochalov, A.G., Tolkachev, M.D., Polekhovsky, Yu.S., Goryacheva, E.M., 2007. Bortnikovite, Pd₄Cu₃Zn, a new mineral species from the unique Konder placer deposit, Khabarovsk krai, Russia. *Geol. Ore Deposits* 49 (4), 318–327.
- Nickel, E.H., 2002. An unusual occurrence of Pd, Pt, Au, Ag and Hg minerals in the Pilbara region of western Australia. *Can. Mineral.* 40, 419–433.
- Nylund, A., 1966. Some notes on the palladium-silicon system. *Acta Chem. Scand.* 20, 2381–2386.
- Oberthür, T., Melcher, F., Gast, L., Wöhrl, C., Lodziak, J., 2004. Detrital platinum-group minerals in rivers draining the eastern Bushveld Complex, South Africa. *Can. Mineral.* 42, 563–582.
- Odile, J.P., Soled, S., Castro, C.A., Wold, A., 1978. Crystal growth and characterization of the transition-metal phosphides copper diphosphide, nickel diphosphide, and rhodium triphosphide. *Inorg. Chem.* 17 (2), 283–286.
- Paar, W.H., Topa, D., Makovicky, E., Sureda, R.J., de Brodtkorb, M.K., Nickel, E.H., et al., 2004. Jagueite, Cu₂Pd₃Se₄, a new mineral species from El Chire, La Rioja, Argentina. *Can. Mineral.* 42, 1745–1755.
- Paar, W.H., Topa, D., Makovicky, E., Culetto, F.J., 2005. Milotaite, a new palladium mineral species from Předbořice, Czech Republic. *Can. Mineral.* 43, 689–694.
- Parthe, E., Hohnke, E., Hulliger, F., 1967. A new structure type with octahedron pairs for Rh₂S₃, Rh₂Se₃ and Ir₂S₃. *Acta Crystallogr.* 23 (5), 832–840.
- Pentek, A., Molnar, F., Tuba, G., Watkinson, D.H., Jones, P.C., 2013. The significance of partial melting processes in hydrothermal low sulfide Cu-Ni-PGE mineralization within the footwall of the Sudbury Igneous Complex, Ontario, Canada. *Econ. Geol.* 108 (1), 59–78.
- Pfann, W.G., 1966. Zone Melting. second ed. John Wiley & Sons, New York, p. 310.
- Pratt, J., 1994. As-Pd-Rh Ternary Phase Diagram Evaluation. In: Effenberg, G. (Ed.), *Phase diagrams, crystallographic and thermodynamic data. Ternary Evaluations*, MSI Eureka MSI, Materials Science International Services GmbH, Stuttgart.
- Predel, B., 1998. Rh-S (Rhodium-Sulfur). Pu-Re-Zn-Zr. Springer Berlin Heidelberg, pp. 1–2.

- Pyon, S., Kudo, K., Nohara, M., 2013. Emergence of superconductivity near the structural phase boundary in Pt-doped IrTe₂ single crystals. *Physica C: Superconductivity* 494, 80–84.
- Rau, H., Rabenau, A., 1968. Hydrothermal growth of some elements. *J. Crystal Growth* 3, 417–421.
- Raub, E., 1954. Über die Reaktion von Silber-Palladium-Legierungen mit Schwefel bei erhöhter Temperatur. *Z. Metallkd.* 45, 533–537, in German.
- Rogers, D.B., Shannon, R.D., Sleight, A.W., Gillson, J.L., 1969. Crystal chemistry of metal dioxides with rutile-related structures. *Inorg. Chem.* 8 (4), 841–849.
- Rossler, F., 1895. Synthese einiger Erzmineralien und analoger Metallverbindungen durch Auflösen und krys-tallisieren lassen derselben in geschmolzenen Metallen. *Z. Anorg. Chem.* 9, 31–77, in German.
- Roy-Montreuil, J., Chaudouet, P., Rouault, A., Boursier, D., Senateur, J.O., Fruchart, R., 1984. Analyse de l'ordre dans les arseniures MMAs. *Ann. Chim.* 4, 411–417, in French.
- Rozhdestvina, V.I., Udovenko, A.A., Rubanov, S.V., Mudrovskaya, N.V., 2016. Structural investigation of cooperite (PtS) crystals. *Crystallog. Rep.* 61 (2), 193–202.
- Rudashevsky, N.S., Kretser, Yu.L., Orsoev, D.A., Kislov, E.V., 2003. Palladium-platinum mineralization in copper-mickel vein ores in the Ioko-Dovyren layered massif. *Doklady Earth Sci.* 391 (6), 858–861, in Russian.
- Rudashevsky, N.S., McDonald, A.M., Cabri, L.J., 2004. Skaergaardite, PdCu, a new mineral platinum-group intermetallic mineral from the Skaergaard intrusion, Greenland. *Min. Mag.* 68 (4), 615–632.
- Ruehl, R., Jeitschko, W., 1982. Preparation and crystal structure of dirhenium pentaphosphide, Re₂P₅, a diamagnetic semiconducting polyphosphide with rhomboidal Re₄ clusters. *Inorg. Chem.* 21 (5), 1886–1891.
- Saini, G.S., Calvert, L.D., Heyding, R.D., Taylor, J.B., 1964. Arsenides og the transitions metals: VII. The Palladium-Arsenic system. *Can. J. Chem.* 42 (3), 620–629.
- Sarah, N., Alasafi, K., Schubert, K., 1981. Kristallstruktur von Pd₂₀Sn₁₃, Pd₆AgPb₄ und Ni₁₃ZnGe₈. *Z. Metallkd* 72 (7), 517–520, in German.
- Savilov, S.V., Kuznetsov, A.N., Popovkin, B.A., Khrustalev, V.N., Simon, P., Getzschmann, J., et al., 2005. Synthesis, crystal structure and electronic structure of modulated Pd_{7-δ}SnTe₂. *Z. Anorg. Allgem. Chem.* 631, 293–301.
- Schafer, H., 1962. *Chemische Transportreaktionen..* Verlag Chemie, MnBh, Weinheim, Bergstr, p. 182. , in German.
- Schneider, A., Esch, U., 1944. Das System Kupfer–Platin. *Z. Elektrochem.* 50, 290–301, in German.
- Schubert, K., Kiefer, B., Wilkens, M., Haufler, R., 1955. On some ordered phases of long period metals. *Z. Metallkd.* 46, 692–715, in German.
- Schwartz, K.B., Gillson, J.L., Shannon, R.D., 1982. Crystal growth of CdPt₃O₆, MnPt₃O₆, CoPt₃O₆ and β-PtO₂. *J. Crystal Growth* 60 (2), 251–254.
- Severson, M.J., Hauck, S.A., 2003. Platinum group elements (PGEs) and platinum group minerals (PGMs) in the Duluth Complex. NRRI, University of Minnesota, Duluth, Technical Report, NRRI/TR-2003/37.
- Shahmiri, M., Murphy, S., Vaughan, D.J., 1985. Structural and phase equilibria studies in the system Pt–Fe–Cu and the occurrence of tulameenite (Pt₂FeCu). *Mineral. Mag.* 49, 547–554.
- Singh, Y., Lee, Y., Nandi, S., Kreyssig, A., Ellern, A., Das, S., et al., 2008. Single-crystal growth and physical properties of the layered arsenide BaRh₂As₂. *Phys. Rev. B* 78 (10), 104512.
- Skinner, B.J., Luce, F.D., Dill, J.A., Ellis, D.E., Hagan, H.A., Lewis, D.M., et al., 1976. Phase realiations in ternary portions of the system Pt–Pd–Fe–As–S. *Econ. Geol.* 71, 1469–1475.
- Sklyarov, E.V., Karyakin, Yu.V., Karmanov, N.S., Tolstykh, N.D., 2016. Platinum-group minerals in dolerites from Alexandra Land Island (Franz Josef Land Archipelago). *Russian Geol. Geophys.* 57 (5), 834–841.
- Sluiter, M.H.F., Colinet, C., Pasturel, A., 2006. Ab initio calculation of the phase stability in Au–Pd and Ag–Pt alloys. *Phys. Rev. B* 73, 174–204.

- Sluzhenikin, S.F., Mokhov, A.V., 2015. Gold and silver in PGE-Cu-Ni and PGE ores of the Noril'sk deposit, Russia. *Mineral. Deposita* 50, 465–492.
- Sluzhenikin S.F., Kozlov V.V., Stanley C.J., Lukashova M.L., Dicks K. Vymazalováite, $Pd_3Bi_2S_2$, a new mineral from the Noril'sk -Talnakh deposit, Krasnoyarskiy region, Russia. *Mineral. Mag. – in press*.
- Soled, S., Wold, A., Gorochov, O., 1975. Crystal growth and characterization of platinum ditelluride. Material. Res. Bull. 10 (8), 831–835.
- Soled, S., Wold, A., Gorochov, O., 1976. Crystal growth and characterization of several platinum sulfoselenides. Material. Res. Bull. 11 (8), 927–932.
- Spiridonov, E.M., Kulagov, E.A., Serova, A.A., Kulikova, I.M., Korotaeva, N.N., Sereda, E.V., et al., 2015. Genetic Pd, Pt, Au, Ag, and Rh mineralogy in Noril'sk sulfide ores. *Geol. Ore Deposits* 57 (5), 402–432.
- Stanley, C.J., Criddle, A.J., Spratt, J., Roberts, A.C., Szymanski, J.T., Welch, M.D., 2005. Kingstonite, ($Rh, Ir, Pt)_3S_4$, a new mineral species from Yubdo, Ethiopia. *Mineral. Mag.* 69 (4), 447–453.
- Stanley, C.J., Vymazalova, A., 2015. Kojonenite, a new palladium tin telluride mineral from the Stillwater Layered Igneous Intrusion, Montana, USA. *Am. Mineral* 100, 447–450.
- Subbotin, V.V., Korchagin, A.U., Savchenko, E.E., 2012. Platinum mineralization of the Fedorova-Pana ore node: types of ores, mineral compositions and genetic features. *Vestnik of the Kola Science Center of the Russian Academy of Sciences, Apatity* 2012 (1), 54–65, in Russian.
- Subramanian, P.R., Laughlin, D.E., 1991. Cu-Pd (Copper-Palladium). *J. Phase Equilibria* 12, 231–243.
- Sugahara, M., Yoshiasa, A., Yoneda, A., Hashimoto, T., Sakai, S., Okube, M., et al., 2008. Single-crystal X-ray diffraction study of $CaIrO_3$. *Amer. Mineral.* 93 (7), 1148–1152.
- Topa, D., Makovicky, E., Balić-Žunić, T., 2006. The crystal structures of jaguéite, $Cu_2Pd_3Se_4$, and chrisstantleyite, $Ag_2Pd_3Se_4$. *Can. Mineral.* 44, 497–505.
- Tsay, M.Y., Chen, S.H., Chen, C.S., Huang, Y.S., 1994. Preparation and characterization of iron-doped RuS_2 single crystals. *J. Crystal Growth* 144 (1), 91–96.
- Tsay, M.Y., Huang, J.K., Chen, C.S., Huang, Y.S., 1995. Crystal growth in tellurium flux and characterization of ruthenium dichalcogenides. *Mater. Res. Bull.* 30 (1), 85–92.
- Vaterlaus, H.P., Bichsel, R., Levy, F., Berger, H., 1985. RuS_2 and $RuSe_2$ single crystals: a study of phonons, optical absorption and electronic properties. *J. Physics C: Solid State Physics* 18 (32), 6063.
- Vymazalová, A., Drábek, M., 2010. The system Pd-Sn-Te at 400°C and mineralogical implications. II. The ternary phases. *Can. Mineral.* 48 (5), 1051–1058.
- Vymazalová, A., Drábek, M., 2011. The Pd–Pb–Te system: phase relations involving pašavaite and potential minerals. *Can. Mineral.* 49 (6), 1679–1686.
- Vymazalová, A., Laufek, F., Drábek, M., Haloda, J., Sidorinová, T., Plášil, J., 2009. Pašavaite, $Pd_3Pb_2Te_2$, a new platinum-group mineral species from Norilsk-Talnakh Ni-Cu camp, Russia. *Can. Mineral.* 47 (1), 53–62.
- Vymazalová, A., Laufek, F., Drábek, M., Cabral, A.R., Haloda, J., Sidorinová, T., et al., 2012a. Jacutingaitaite, Pt_2HgSe_3 , a new platinum-group mineral from the Caué iron-ore deposit, Itabira District, Minas Gerais, Brazil. *Can. Mineral.* 50 (2), 431–440.
- Vymazalová, A., Laufek, F., Drábek, M., Stanley, C.J., Baker, R.J., Bermejo, R., et al., 2012b. Zaccariniite, $RhNiAs$, a new platinum-group mineral species from Loma Peguera, Dominican Republic. *Can. Mineral.* 50, 1321–1329.
- Vymazalová, A., Chareev, D.A., Kristavchuk, A.V., Laufek, F., Drábek, M., 2014b. The system Ag-Pd-Se: phase relations involving minerals and potential new minerals. *Can. Mineral.* 52, 77–89.
- Vymazalová, A., Grokhovskaya, T.L., Laufek, F., Rassulov, V.I., 2014a. Lukkulaisvaaraite, $Pd_{14}Ag_2Te_9$, a new mineral from Lukkulaisvaara intrusion, northern Russian Karelia, Russia. *Mineral. Mag.* 78 (7), 1491–1502.
- Vymazalová, A., Laufek, F., Kristavchuk, A.V., Chareev, D.A., Drábek, M., 2015. The system Ag-Pd-Te: phase relations and mineral assemblages. *Mineral. Mag.* 79 (7), 1813–1832.

- Vymazalová, A., Laufek, F., Sluzhenikin, S.F., Stanley, C.J., 2017. Norilskite, $(\text{Pd},\text{Ag})_7\text{Pb}_4$, a new mineral from Norilsk -Talnakh deposit, Russia. *Mineral. Mag.* 81 (3), 531–541.
- Vymazalová, A., Laufek, F., Sluzhenikin, S.F., Stanley, C.J., Kozlov, V.V., Chareev, D.A., et al.: Kravtsovite, PdAg_2S , a new mineral from Norilsk -Talnakh deposit, Krasnoyarskiy kray, Russia. *Eur. J. Mineral.* in press.
- Wilke, K.T., 1973. Kristallzüchtung. Harri Deutsch Verlag 600, in German.
- Yen, P.C., Chen, R.S., Chen, C.C., Huang, Y.S., Tiong, K.K., 2004. Growth and characterization of OsO_2 single crystals. *J. Crystal Growth* 262 (1), 271–276.
- Yu, Z., Cheng, F., Ma, H., 2009. Lisiguangite, CuPtBiS_3 , a New Platinum-Group Mineral from the Yanshan Mountains, Hebei, China. *Acta Geologica Sinica* 83 (2), 238–244.
- Zhang, W., Yanagisawa, K., Kamiya, S., Shou, T., 2009. Phase Controllable Synthesis of Well-Crystallized Rhodium Sulfides by the Hydrothermal Method. *Crystal Growth Design* 9 (8), 3765–3770.
- Zhuravlev, N.N., 1976. Physicochemical investigation of some superconducting alloys in the System Pd-Pb-Bi (Sections PdBi-PdPb and $\text{PdBi}_2\text{-PdPb}_2$). *Vestn. Mosk. Univ., Ser. 3: Fiz. Astron* 17, 392–396.